SECTION 3

INJECTION SYSTEM

3.1. Introduction

If 10^{12} protons per pulse is to be attained in Nimrod it could be necessary to inject about 10^{14}, most of which will, of course, be lost even before acceleration begins. The injection system has accordingly been designed to yield at least 20 mA for a maximum pulse length of 1.5 ms. This injection time corresponds to a lower limit of $\dot{B}$ at injection of 2 kG/s. Optimum injection conditions cannot be predicted since they will depend on phase space current density distribution of the 15 MeV beam and space charge effects in the synchrotron. It is anticipated however that the optimum will be covered by the available range of the parameters concerned.

The injection system is shown in Fig. 3.1(i); it might almost be described as conventional in its functional conception. The main parameters are listed in section 1, Table 1(I).

The 15 MeV linear accelerator is a strong focused Alvarez structure running at 115 Mc/s. Its output energy was determined after consideration of gas scattering losses and remanent field effects in the synchrotron, on the one hand, and complexity, cost and electrostatic inflector breakdowns on the other. Pre-injection energy, initial aperture desired, attainable quadrupole gradient in the first drift tube, and commercially available power valves were all considered in fixing the operating frequency.

An achromatic inflector is necessary for efficient injection of the 15 MeV beam, even assuming the debuncher to be working satisfactorily, and also serves to convey the beam past certain obstructions to a simple inflection arc.

Quadrupoles in the low and high energy drift spaces (LEDS and HEDS) are arranged to transport the beam and match it, over a range of input and output conditions. Beam current transformers (B.C.T.s), fluorescent screens, stops, foils and "Faraday cups" are introduced into the flight tube as required and a "4 jaw box" system allows beam definition by edges, slits, apertures etc. As a general rule, every 4 jaw box has a B.C.T. on either side of it. The B.C.T.s are integral with the flight tube for the most part, other components such as screens and stops are on reciprocating shafts and mounted on standard probe boxes.

Table 3.1(I) summarises the injector history.

TABLE 3.1(I) INJECTOR HISTORY

September 1957	First major contract for the 650 kV installation placed.
March 1959	650 kV equipment received on site.
August 1959	Construction of the pre-injector completed.
December 1959	First accelerated beams achieved from the pre-injector. Vacuum tank for the linac received.

TABLE 3.1(I) INJECTOR HISTORY (Contd.)

January 1960	Main r.f. valve, RS1041, received.
February 1960	Modulator for r.f. drive chain received.
July 1960	Linac cavity received.
March 1961	Last of the linac drift tubes, which were delivered over a period of nine months, received.
May 1961	Last drift tube installed. First vacuum test on the completed linac.
1st July 1961	High r.f. power fed into the linac for the first time.
1st August 1961	First successful acceleration to 15 MeV.

The first 15 MeV beam was obtained on 1st August, 1961, and intermittently during the following six weeks. Some basic measurements, e.g. threshold and trapping efficiency were made and much equipment proved, but operating conditions deteriorated continually, the main difficulties being sparking and multipactoring in the linac and sparking in the main power amplifier circuit. After effecting improvements and repairs to the valve circuit and cleaning up the linac drift tubes, operation was once more attempted in October but multipactoring dominated the situation until February, 1962, when the drift tube faces were lampblacked. This completely stopped multipactoring although a painstaking conditioning phase was now required against sparking. Very satisfactory running conditions obtained until June was an effective, although temporary repair realised. Since then good running has been experienced with one interruption for cleaning drift tube faces to reduce the incidence of sparking.

Installation in the LEDS and HEDS in anything like final form has been deliberately delayed to allow for as much detailed study as possible of the beam properties. This work though still incomplete, has been of great value in helping to understand the beam physics and in deciding upon a detailed component layout. Measurements are made of, for example, current proton percentage, emittance, and momentum distribution.

This report takes account of events up to the end of 1962.

3.2. Dynamics of the Injector

3.2.1. Dynamical Design of the Linac

(a) Preliminary work

It was decided at an early stage to adopt alternating gradient quadrupoles for the injector as this was the most obvious way of ensuring the highest accelerated currents. A number of experimental quadrupoles were constructed as a guide to magnetic and electrical design. The outcome of this work was the determination of a maximum practicable quadrupole gradient and a corresponding aperture. From an elementary consideration of the dynamical stability of accelerated particles, together with knowledge of the frequency dependence of electrical breakdown it was possible to specify a relationship between initial particle energy and frequency, appropriate to this estimated maximum quadrupole gradient (1).

Subject to this relationship the choices of frequency and injection energy were 115 Mc/s and 600 keV respectively, the latter being consistent with experience of Cockcroft-Walton accelerators and the availability of high voltage power supplies. The output energy of 15 MeV was chosen by weighing the difficulty of producing an inflection system for higher energy particles against their more favourable gas-scattering loss factor. It was also compatible with the minimum useful magnetic field obtainable in the synchrotron.

The effect of misalignment of the quadrupoles was investigated to determine a rate of increase of aperture which would make the probability of particle loss equal at all points through the machine. The maximum initial rate of increase was determined independently by the required quadrupole gradient variation. On this basis the misalignment investigation specified the aperture throughout the machine, together with alignment tolerances for the quadrupoles. As a result of these preliminary calculations it was also possible to specify the approximate length of the machine, the mean accelerating field and the number of unit cells (Fig. 3.4.8(i)). Resonance experiments on scaled unit cells were used to specify the geometry of a unit cell at any point in the machine in terms of the corresponding particle velocity.

(b) Final Dynamical Design

The final stage in the dynamical design was an extensive computation on a Mercury computer, aimed at specifying an actual number of unit cells and then precise dimensions, consistent with the other required features of the design (2). It was assumed that a "reference particle" must cross from the centre of one unit cell to the centre of the next in exactly one r.f. cycle. The r.f. phases at which successive cell centres are passed are thus separated by 2 radians i.e. this occurs at a constant reference phase with respect to each r.f. cycle. The entry and exit phases can be stated with respect to this in terms of the input and output velocities. The computation proceeded by calculating the motion of a particle through a unit cell, its dimensions being appropriate to the input velocity. This established a certain output velocity which was used to define the dimensions of another unit cell for which the particle motion was again computed. In neither of these unit cells was the output phase correctly related to the reference phase and output velocity, but by linear interpolation a unit-cell with the correct relationship could be found. This was used as the starting point for a computation of the following unit cell, and so on throughout the linac. By computing a number

of complete accelerators with differing electrical field-strengths and interpolating, a final design was obtained which incorporated all the requirements to an acceptable accuracy.

On the basis of this design further computation of beam acceptances were made for each of the two planes of symmetry and for a number of input phases and energies (3). Radial and phase motion were also examined in some detail and the effect of a buncher was considered (3). Finally a computation was made of the effect of rotational misalignment of the quadrupoles on beam acceptance (4).

3.2.2. Drift Spaces

The low energy drift space (LEDS) constitutes a matching system between the 600 keV pre-injector and the linac. Provision is made for a "four parameter match" that is the realisation of two required beam conditions, say beam radius and slope, in each of the two planes of symmetry. This necessitates control of four variables in the matching system which in fact are the total and out-of-balance energising currents in each of two quadrupole triplets. There is a third triplet downstream of these two and very close to the linac input, its function being to handle the rather drastic transition between the low gradient matching system and the high gradient linac focusing system. This third triplet must also be compatible with the passing of a fairly small diameter beam through the buncher, the component which is immediately upstream from it. Its energisation is intended to be permanently set at levels which conform to these requirements.

The focusing components of the high energy drift space (HEDS) form essentially two double triplet matching systems in series separated by a fairly long drift space containing the debuncher. The first matching system must be capable of transforming the linac output beam in such a way that it passes with radial and axial symmetry through the debuncher at any position in the central drift space. The second system must be able to transform the symmetrical beam from the debuncher to a variety of conditions dictated ultimately by a range of input radii to the synchrotron which gives a corresponding range of focal properties to the inflector.

3.2.3. Buncher and Debuncher

The buncher imparts an energy modulation to the 600 keV beam at the linac frequency. The position at which the bunch occurs is determined by the axial beam velocity and the depth of the modulation, and when this is fixed, the time at which the bunch occurs relative to the linac field is determined by the buncher phase. The magnitudes and stability of these three quantities have been related to the phase-energy acceptance of the linac in such a way as to ensure a substantial and stable gain in accepted charge.

The debuncher imparts an energy modulation to the 15 MeV beam after the energy spread in the beam has brought about some axial resolution travelling along the HEDS.

Particles of higher energy reach the debuncher before those of lower energy, hence by correct phasing of the debuncher field the early ones may be accelerated and the late ones decelerated, the result being a much narrower energy spectrum.

The post-acceleration drift length and the debuncher field have been chosen to give optimum debunching for estimated energy-phase characteristics of the 15 MeV beam.

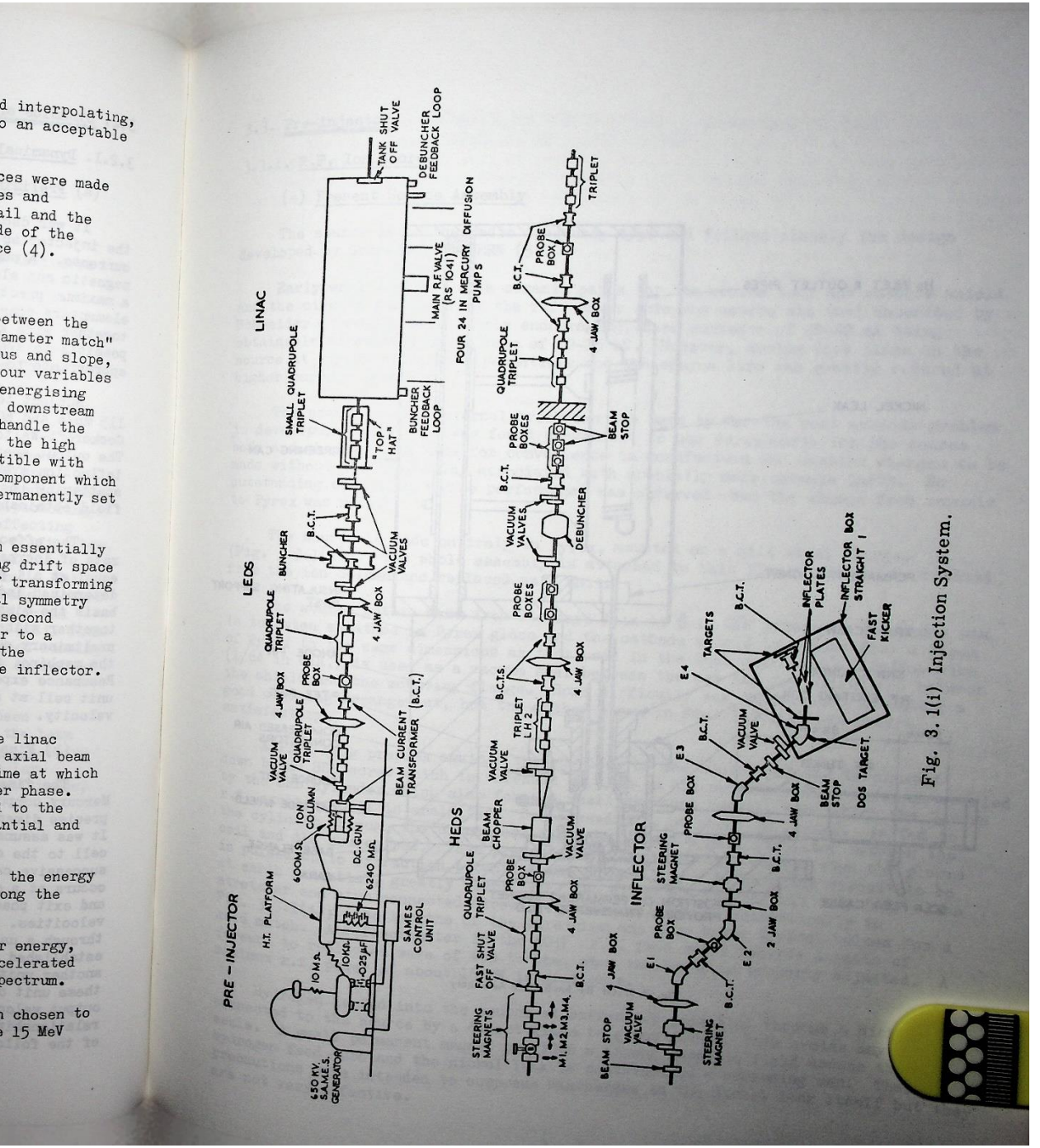

Fig. 3.1(i) Injection System.

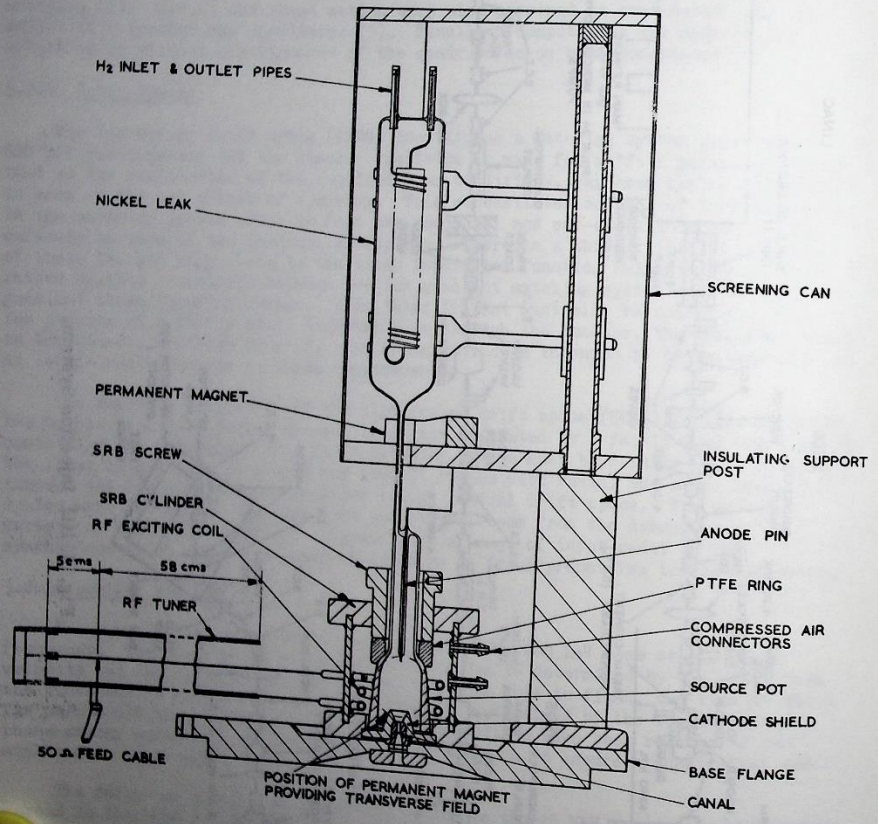

Fig. 3.3.1(i) RF Ion Source Assembly

3.3. Pre-injector

3.3.1. R.F. Ion Source

(a) Present Source Assembly

The source is of the radio frequency type and follows closely the design developed by Schneider at CERN (5).

Early work was done with ceramic parts for the source body and cathode shield and the circuit for coupling the r.f. power into the source was that described by Schneider. Results were fairly encouraging, beam currents of 30-40 mA being obtainable at extraction voltage of 10-15 kV. However, arcing took place in the source at higher extraction potentials and the source life was greatly reduced at higher current levels.

The phenomenon of internal breakdown has been by far the most serious problem in development work. It was found convenient to use Pyrex parts for the source body and shield which made for convenience in manufacture and enabled changes to be made without the long delay associated with specially made ceramic parts. No outstanding change in source performance was observed when the change from ceramic to Pyrex was made.

The source is made entirely in Pyrex, mounted on a mild steel flange, (Fig. 3.3.1(i)). The whole assembly is attached to this flange and can be removed from the ion column and replaced as a unit.

The source pot is made from standard 1 in to $\frac{5}{8}$ in QVF reducer. The anode pin is tungsten sheathed in Pyrex glass and the cathode shield is ground from a block of Pyrex to the same dimensions as that used in the CERN source (5). Indium wire (1/64 in dia.) is used as a vacuum seal between the pot and the shield and between the shield and the mounting flange. Some difficulty was experienced in making a good clamping arrangement, but the method shown in Fig. 3.3.1(i) has proved satisfactory.

A PTFE ring presses against the shoulder of the source pot and is clamped down by an SRB screw which is threaded 40 t/in on the outside. This screw is carried by the SRB cylinder which also forms a small pressure vessel, into which the 2 turn r.f. exciting coil is araldited. Compressed air, at about 30 lb/in^2, is fed to the cylinder through the connectors shown and forms a good insulator between the coil and the source pot. This prevents discharges in this region when the plasma is pulsed up to extraction potential and enables the r.f. matching circuit to be at earth potential, greatly simplifying the circuit. The circuit is a 50 Ω line stretcher and stub connected directly to the coil, shown schematically in Fig. 3.3.1(i); the lengths of the stretcher and stud being typical values for a good match. A reflectometer in the 50 Ω r.f. feed cable records a ratio of forward to reflected wave of ten to one, when the tuner is properly adjusted. A maximum r.f. power of about 15 kW is available.

Hydrogen is fed into the source at extraction potential through a nickel leak connected to the source by a direct glass to glass joint. This avoids any 'O' ring seals. A small permanent magnet provides a strong magnetic field across the hydrogen feed tube and the nickel leak is contained in a screening can. These precautions were intended to suppress discharges in the nickel leak itself but they are not very effective.

The exit canal dimensions are 3.5 mm dia. and 8 mm long in the parallel part and it is located in an accurately turned recess in the base flange. It was accidentally made in mild steel and, since it seems to give no obvious trouble, the material has not been changed. Two permanent magnets provide a transverse magnetic field of about 50 gauss in the source pot which increases the ion density at a given r.f. power.

The maximum output so far obtained from this source in service, is about 100 mA with 20 kV extraction potential, and r.f. power very roughly 10 kW and a pulse length of 170 μs (r.f. pulse length 700 μs). This was measured by a beam toroid after acceleration to 600 kV and represents the total beam current. After operation for about half an hour at this level the source failed by arcing internally. The source has operated at 20-30 mA for about 200 h so far without trouble.

The sources are operated on a laboratory rig and their performance checked before being used on the injector. A typical graph of total output current against extraction voltage is shown in Fig. 3.3.1(ii). The r.f. power level is optimised at each value of extraction voltage and the beam current is measured with a collector cup having a transverse magnetic field to suppress secondary electrons.

(b) Operational Experience

Internal Arcing

When the extraction voltage is raised above about 15 kV there is the possibility of internal breakdown leading to an arc discharge. This effect has been by far the most difficult and intractible problem in the development of the source. It has been very difficult to find any parameter which affects the phenomenon in a consistent manner.

The one clear cut result to emerge is the effect of impurities in the discharge in initiating breakdown. In early work with Pyrex sources, they were stuck together with Araldite and suffered very badly from internal arcing. Since then, great care has been taken to clean and dry the glass parts thoroughly and all 'O' rings and Araldite have been eliminated. The arcing has been much less troublesome though the problem is by no means completely solved.

The glass parts are washed in concentrated nitric acid then in dilute hydrofluoric before being thoroughly rinsed in tap water followed by distilled water. They are dried in an oven at about 150°C for several hours. On one or two occasions the hydrofluoric acid has been concentrated enough to etch the glass slightly and this seemed to give a poor source.

There have been two periods when the source performance on the Injector deteriorated for no apparent reason. Eventually in both cases contamination was thought to be the cause. In the first instance the glass parts had not been sufficiently thoroughly dried and in the second, leaks were found which allowed small amounts of air into the discharge. The leaks were never large enough to show up on the ion gauges of the ion column.

Arcing also occurs much more readily on long pulses. A source which is working well with a pulse length of about 100 μs for example, will often start to breakdown when the pulse length is increased to 1 ms. Persistent arcing can cause

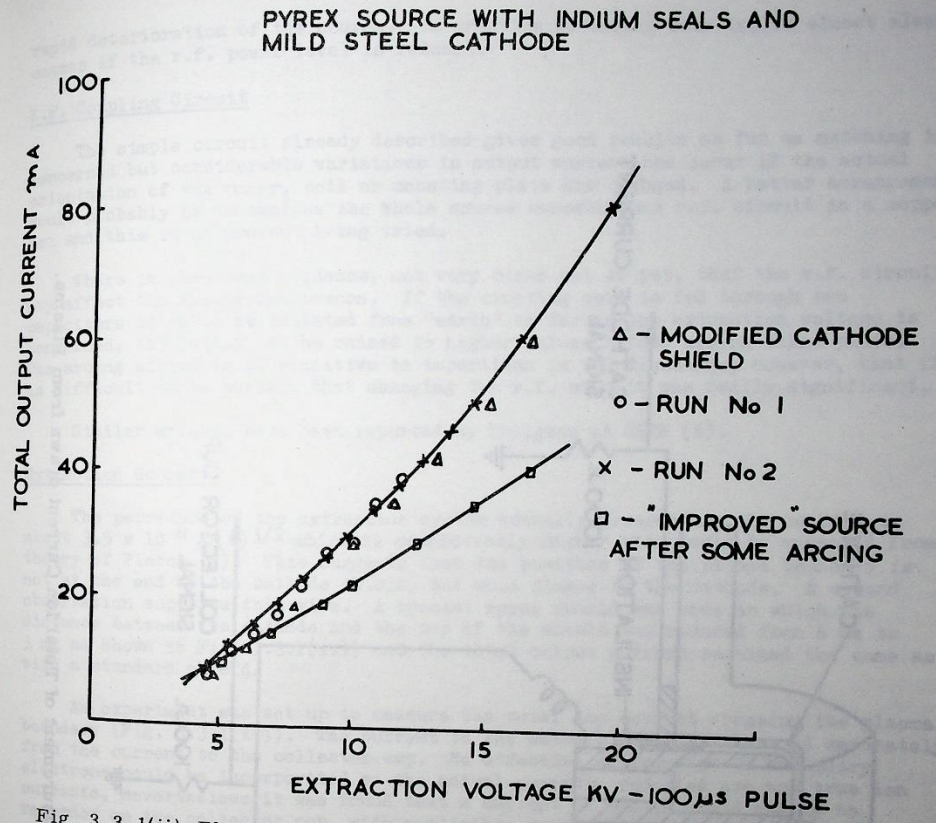

Fig. 3.3.1(ii) Plot of Ion Source Output Current against Extraction Voltage.

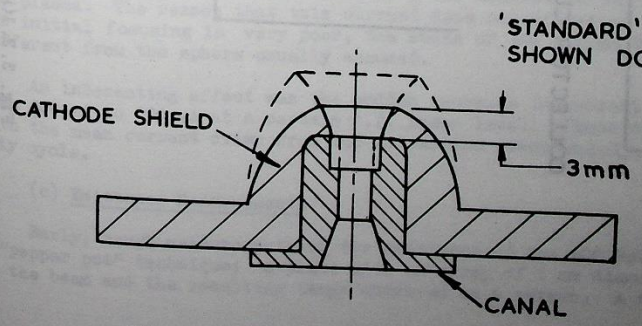

Fig. 3.3.1(iii) Ion Source Short Cathode Shield.

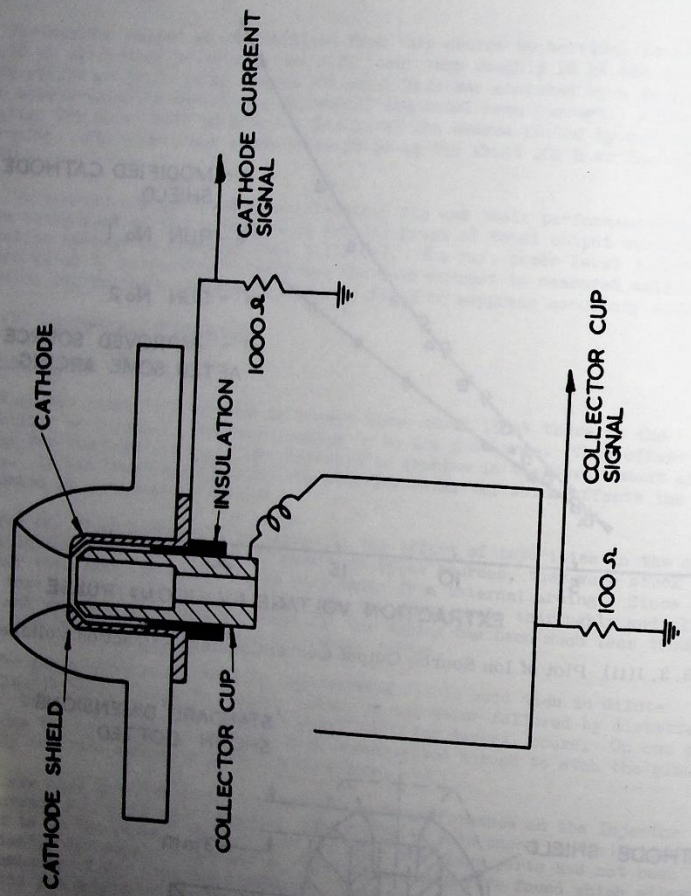

Fig. 3.3.1(iv) Measurement of Total Ion Current drawn from Plasma.

rapid deterioration of the source. In practice if arcing sets in, it almost always ceases if the r.f. power level is reduced.

R.F. Coupling Circuit

The simple circuit already described gives good results as far as matching is concerned but considerable variations in output current can occur if the actual orientation of the tuner, coil or mounting plate are changed. A better arrangement would probably be to enclose the whole source assembly and r.f. circuit in a copper box and this is at present being tried.

There is also some evidence, not very clear cut as yet, that the r.f. circuit may affect the arcing phenomenon. If the exciting coil is fed through two capacitors so as to be isolated from "earth" as far as the extraction voltage is concerned, the latter can be raised to higher values before arcing takes place. The arcing effect is so sensitive to impurities in the discharge, however, that it is difficult to be certain that changing the r.f. circuit was really significant.

Similar effects have been reported by Tallgren at CERN (6).

Extraction Geometry

The perveance of the extraction system actually observed on the machine is about 3.5×10^{-8} A/(V)$^{3/2}$ which is considerably higher than would be expected from the theory of Pierce (7). This suggests that the position of the plasma boundary is not at the end of the cathode shield, but much closer to the cathode. A second observation supports this view. A special Pyrex shield was made in which the distance between the cathode and the top of the shield was reduced from 6 mm to 3 mm as shown in Fig. 3.3.1(iii) and the total output current remained the same as with a standard shield.

An experiment was set up to measure the total ion current crossing the plasma boundary (Fig. 3.3.1(iv)). The current to the cathode could be measured separately from the current to the collector cup. No effective suppression of secondary electrons could be incorporated so the actual currents recorded are not true ion currents, nevertheless it was found that a current of 500 mA could easily be recorded on the collector cup, with negligible current to the cathode, at an extraction voltage of a few kV.

Thus it seems that ion currents of a few hundred mA can easily be drawn from the plasma. The reason that this current does not appear as useful beam may be that the initial focusing is very poor, the shape of the plasma boundary being far different from the sphere usually assumed.

An interesting effect was the sudden increase in current to the collector cup from 200 mA to 500 mA at a certain r.f. power level. These currents were consistent with the mean current drawn from the extraction power supply, allowing for the duty cycle.

(c) Emittance Measurements

Early, rough measurements of the emittance of the 600 keV beam were done with a "pepper pot" technique; a plate with an array of 1 mm diameter holes was placed in the beam and the resulting image observed on a screen. A few measurements were

made by allowing the beam transmitted by the pepper pot to fall on a copper plate coated with MbO. This was too slow a method, although a clear image could be obtained with a few beam pulses and even a single pulse produced a visible image. Later a quartz screen was used together with a polaroid camera for quick results. The emittance was found to be between 2 and 5 mrad cm for most conditions.

An interesting feature of these measurements was the complexity of the images which could be obtained. Sometimes two or more distinct 'spots' could be seen corresponding to a single pin hole in the pepper pot plate. When a transverse magnetic field was applied (downstream from the pepper pot) the separate 'spots' were deflected equally and resolved into ions of different mass in the same way showing that each spot contained ions of all species.

Later, a much more detailed measurement was performed using two remotely controlled, 4 jaw apertures. The upstream box was set to a 1 mm^2 aperture and for each radial position of this the transmitted beam was scanned by a 1 mm slit in the downstream 4 jaw aperture. The current through this slit was measured by a collector plate having a transverse magnetic field to suppress secondary electrons. Thus a curve of current distribution, in the divergence co-ordinate was found for each radial co-ordinate. Fig. 3.3.1(v) and Fig. 3.3.1(vi) show emittance diagrams for the vertical and horizontal planes.

It is clear that the current distribution in phase space is by no means uniform and that most of the beam is in a smaller phase space area than the 'total' emittance. The emittance boundaries shown in Fig. 3.3.1(v) and Fig. 3.3.1(vi) were obtained by drawing through the points on the current distribution curves at which the current had fallen to 5% of the total.

Some of the current distribution curves have double peaks. A rough mass analysis of the beam downstream from the first 4 jaw aperture showed that the larger peak was made up of protons while the smaller one was due to molecular ions. Thus it seems that the 'double peak' effect is different from the 'double spot' effect mentioned above. The molecular ions may have been separated out by a triplet quadrupole which was used in the experiment.

(d) Proton Percentage

The proton percentage measured in the centre of the 600 keV beam is about 85% with a good source. When the source has been contaminated the percentage has fallen to below 50% and on one source assembly, which had a vacuum leak, the proton percentage was only 40% while about a third of the beam was made up of heavy ions, probably oxygen and nitrogen.

3.3.2. Ion Column

The construction of the column is closely similar to that described in (8), with the electrodes made in stainless steel rather than aluminium. The focusing electrodes are as shown in Fig. 3.3.2(i).

It is pumped by a mercury diffusion pump with a refrigerated chevron baffle and liquid nitrogen cold trap. The normal base pressure measured on an untrapped ion gauge is about 5 x 10-6 torr. With the source in operation this rises to about 2 x 10-5 torr.

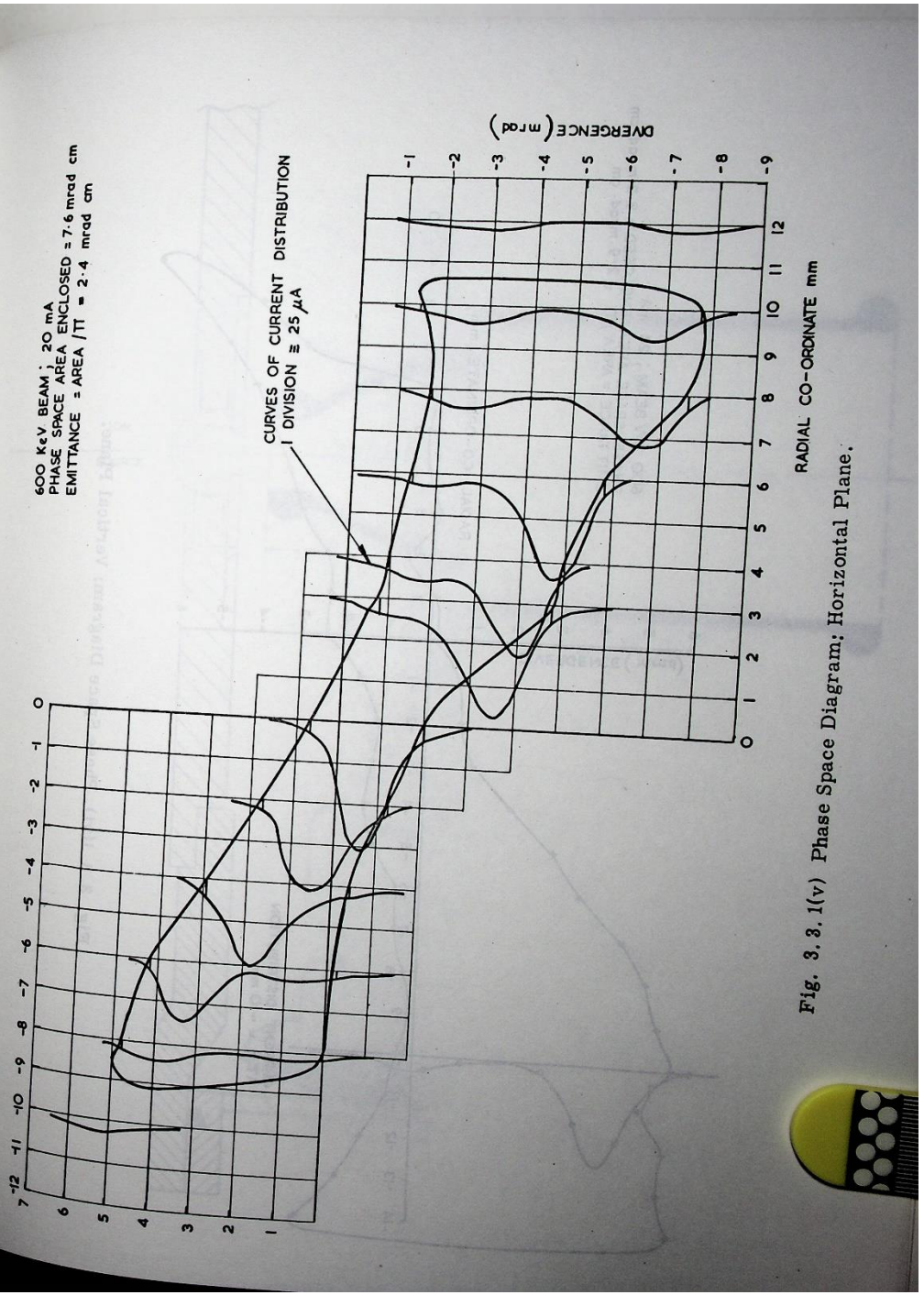

Fig. 3.3.1(v) Phase Space Diagram: Horizontal Plane.

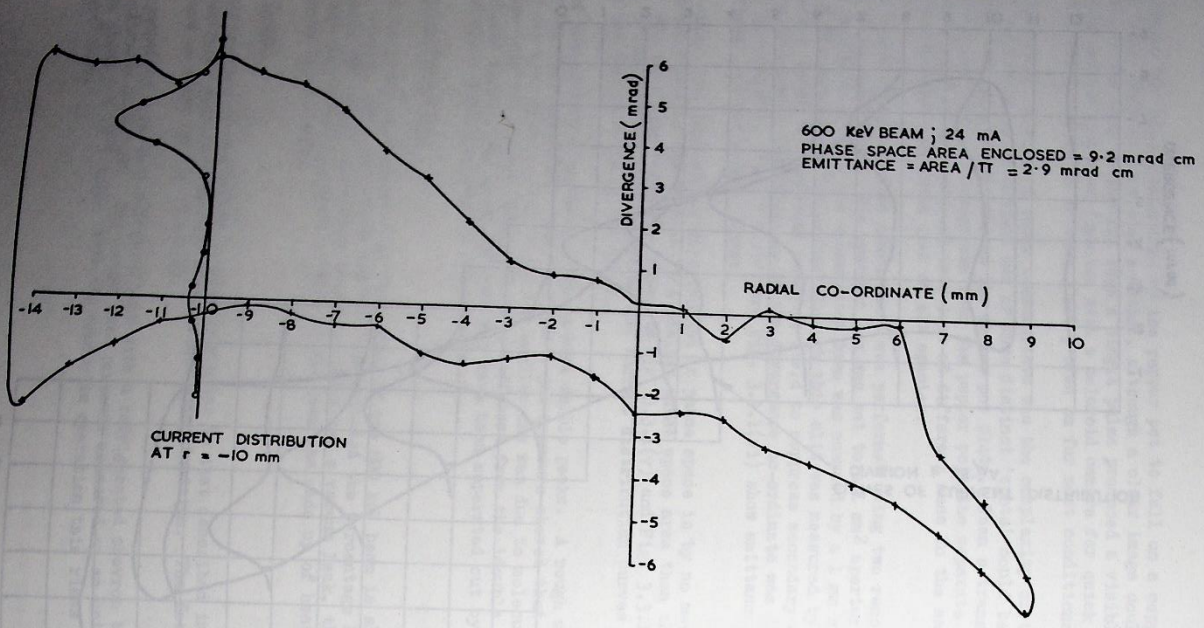

Fig. 3.3.1(vi) Phase Space Diagram: Vertical Plane.

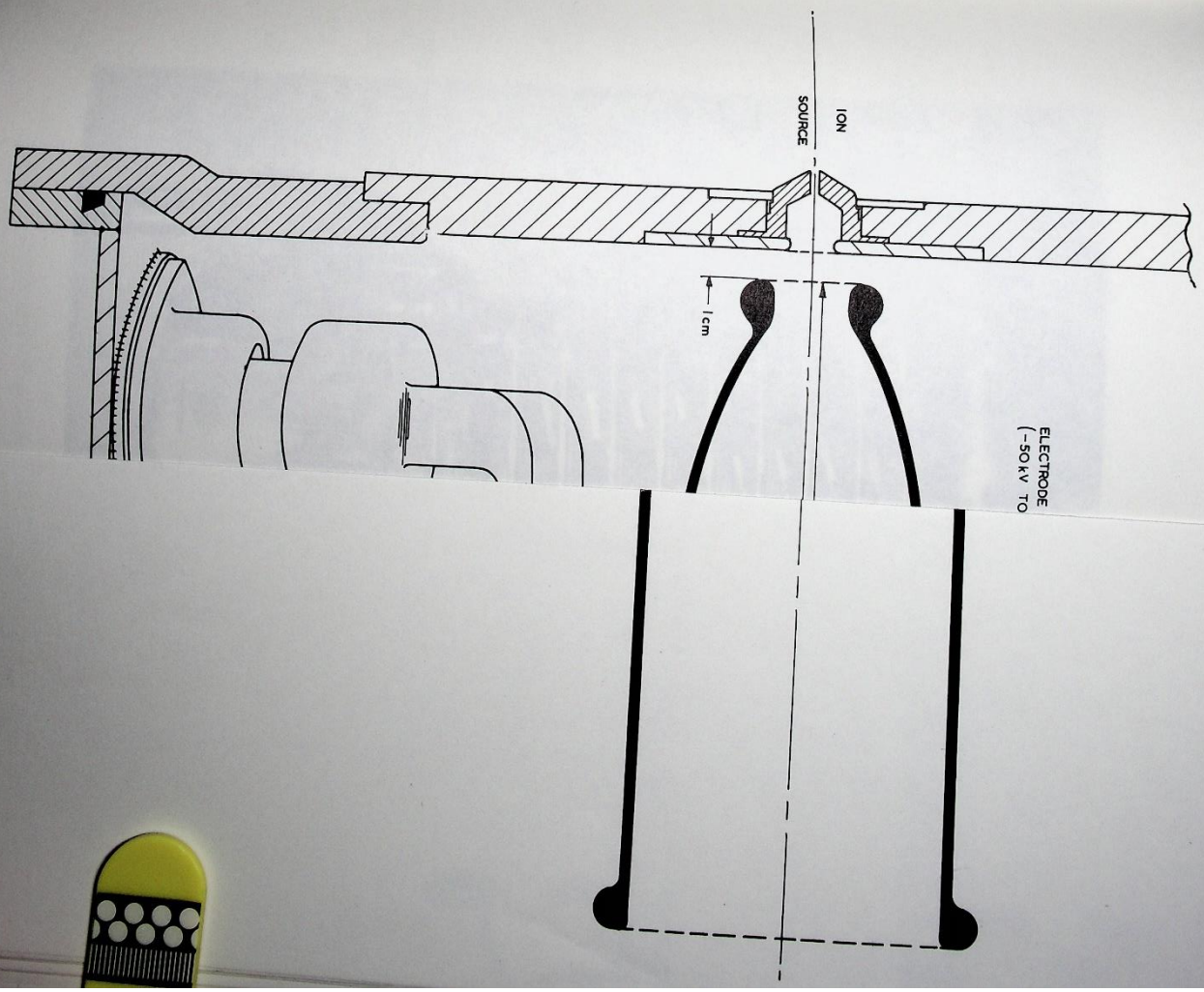

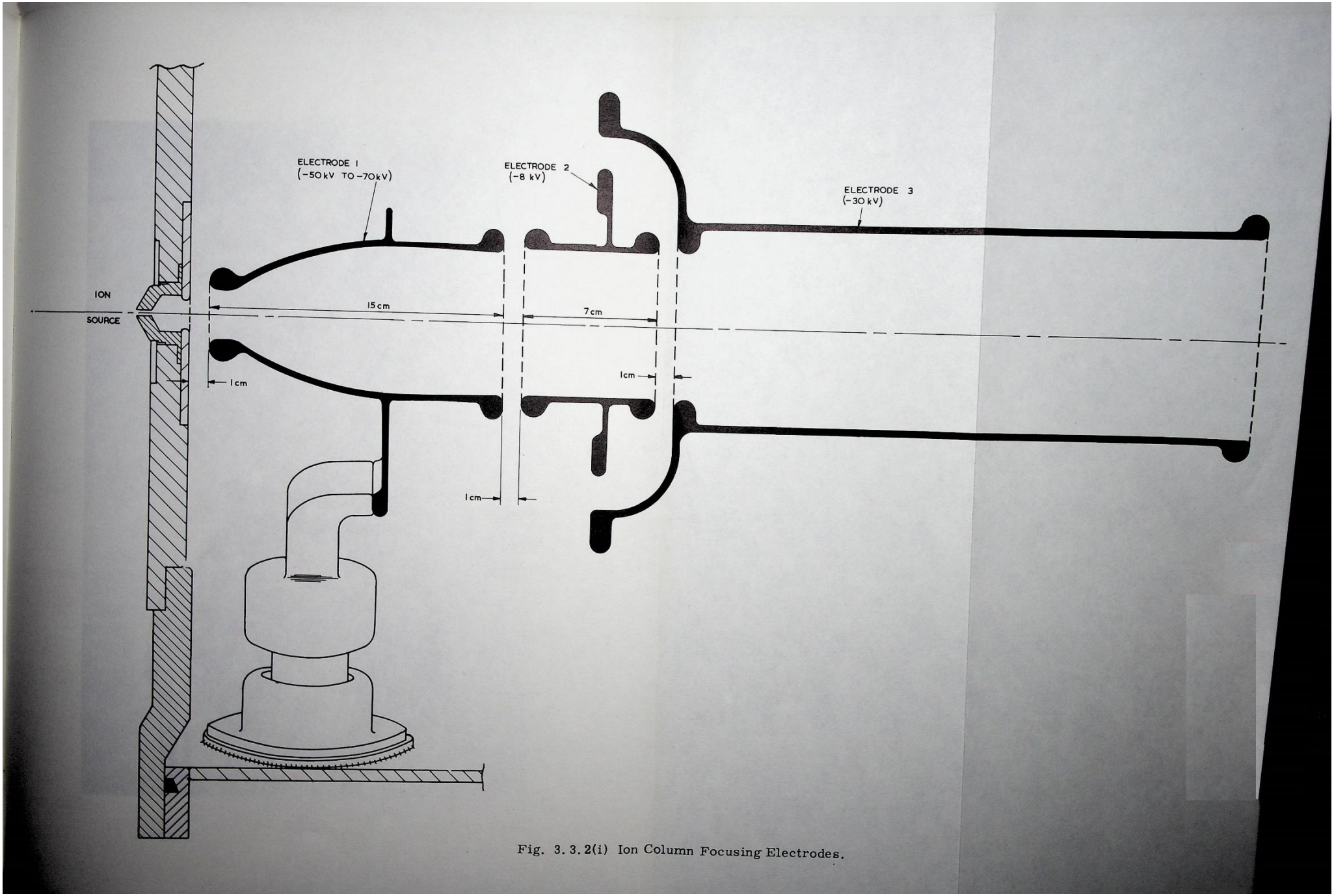

Fig. 3.3.2(i) Ion Column Focusing Electrodes.

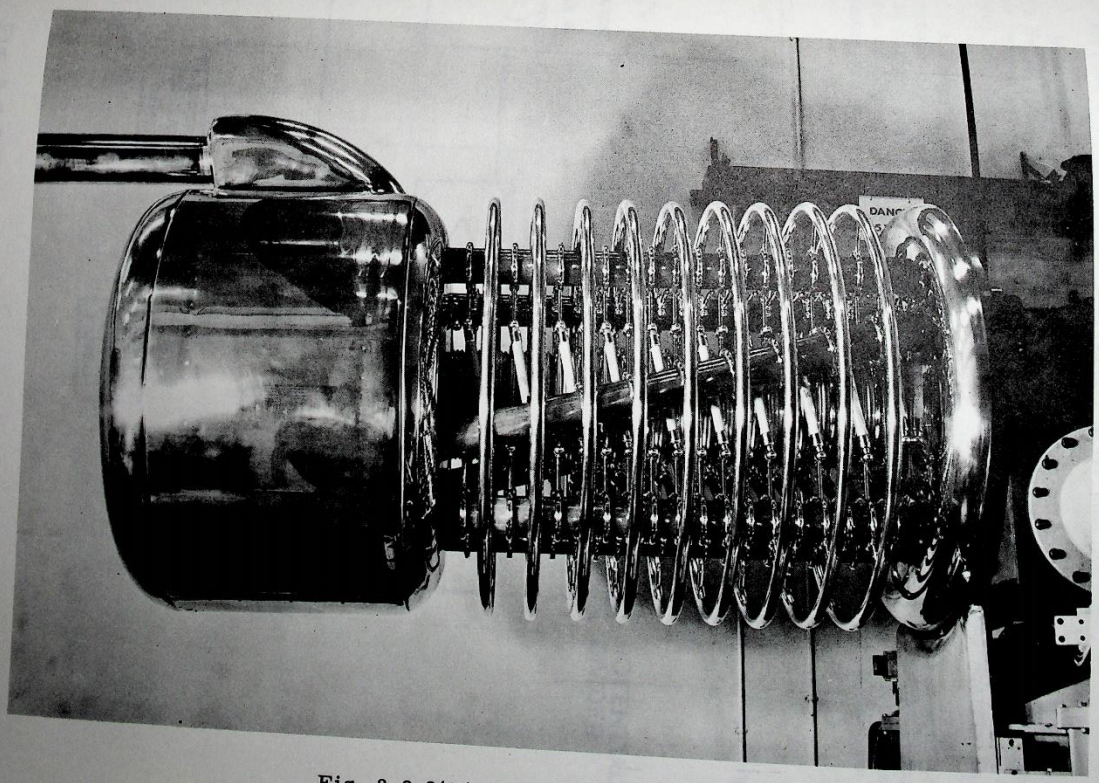

Fig. 3.3.2(ii) View of the Ion Column.

The initial conditioning of the column was a tedious process spread over about two weeks but no trouble is experienced at the present time. When the column has been let up to atmospheric pressure, to change a source unit for example, 600 kV can be applied without trouble immediately after pumping down.

When beams of 20–30 mA at pulse lengths of about 100 μs are being accelerated, the X-ray production, indicated by a type 1349 hand monitor, is less than 2 mr/h at the nearest point to the column outside the safety screen. With beam currents of about 50 mA for pulse lengths of 1 ms the X-ray level rises sharply to over 50 mr/h.

A large cylindrical electrode in the pumping manifold is biased to -500 V to suppress secondary electrons. No trouble is experienced with 100 μs pulses, but with higher intensity beams of 1 ms pulse length the column requires an additional chain of 1500 pF capacitors to stabilise the electrode potentials. No extended running has yet been done with long beam pulses.

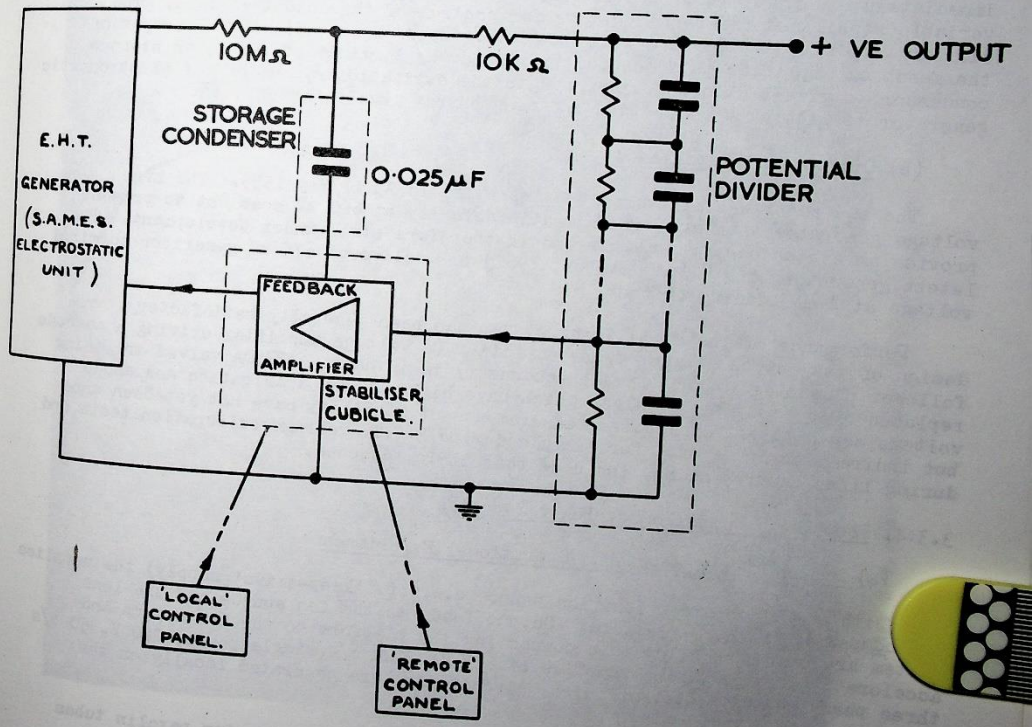

Fig. 3.3.3(i) Schematic Diagram of 600kV DC Supply System.

3.3.3. Ion Column Power Supply

(a) Present System

The requirement was to provide a 650 kV maximum positive polarity output, 4 mA maximum mean D.C. supply capable of remote control. With pulse current loading up to a maximum of 200 mA, 2 ms pulsed at 2 pulses/s, the output voltage was to be within ±1.5 kV during pulses.

The equipment consists of an electrostatic generator whose output is connected to a 25 nF storage condenser via a charging and surge protecting resistor. The value of this resistor has been changed from an initial 3.5 M Ω to 10 M Ω (Fig. 3.3.3(i)). Connection to the H.T. platform, which houses the focusing and ion source supplies, and to the d.c. accelerator column, is via a 10 K Ω discharge current limiting resistor designed and manufactured locally. The final output voltage is measured by a resistance-capacitance divider connected to the H.T. platform and situated immediately underneath it. The low potential end of the divider is returned to a variable stabilised reference voltage for control of the output voltage. The divider tapping point feeds a wide band d.c. feedback amplifier. The output of the feedback amplifier is connected to the earthy terminal of the 25 nF storage condenser to give fast correction, and to the excitation system of the electrostatic generator to give slow correction and mean output level control.

(b) Operational Experience

The equipment was delivered and installed in April/May 1959. The high voltage generator although working satisfactorily at 600 kV does not at present provide an adequate safety margin and is therefore still under development. The latest generator (installed October, 1962) has delivered 675 kV generator terminal voltage at 4 mA loading on test.

Performance of the stabilising system has been generally satisfactory; redesign of the output stages of the amplifier (a voltage amplifier driving a cathode follower connected to the storage condenser) is in hand. 4PR60A valves are being replaced by type 4PR250C valves which have higher power dissipation and anode voltage capability. Exhaustive measurements of stability have not yet been done but indirect observations, for example during E.H.T. voltage calibration tests and during linac commissioning, indicate that it is adequate.

3.3.4. Focusing and Ion Source Power Supplies

(a) Present arrangement and Operational Experience

With one minor exception (ion source c.w.r.f. 'keep-alive' supply) the supplies are housed on the H.T. platform: Output leads to the ion source and the lens system are run in an alloy tube connecting the platform to the ion source and accelerator column. Mains supplies of 115 V, 2000 c/s single phase, 220 V, 50 c/s three phase and 24 V d.c. (control circuit use) are generated locally on the platform.

The platform is insulated from ground by four 18 in diameter paxolin tubes which also provide mechanical support. The tubes house respectively:-

i) Insulating shaft drive from a motor at earth potential for the platform generators,

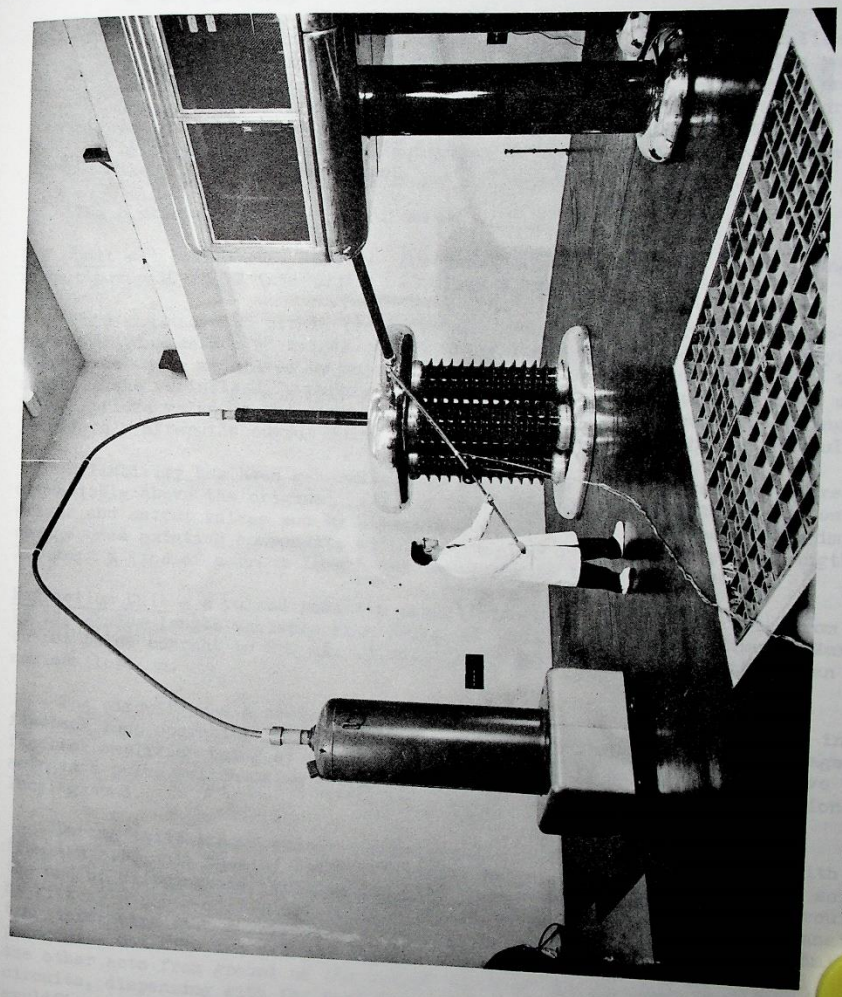

Fig. 3.3.3(ii) View of E.H.T. Generator, Condenser and H.T. Platform.

ii) Four 1 in dia. perspex rod light guides for timing pulse control and pulse monitoring,

iii) Polythene tubes for filtered cooling air which is piped to the major units on the platform,

iv) P.V.C. tubes carrying compressed air which is used for operation of air switches providing unit ON/OFF and signal back circuits; ten paxolin tube rotary drives for Variacs and potentiometers controlling unit output levels. There is also P.V.C. tubing carrying compressed air for ion source cooling and insulation, and polythene tubing for the ion source hydrogen feed. Terminal equipment is housed in a cellar immediately under the platform support legs.

The platform units are as follows:-

R.F. Unit - a pulsed r.f. supply; frequency 125 Mc/s nominal; pulse length 2 ms; output power 10-15 kW into 50 Ω ; 2 pulses/s maximum.

This was designed within the group and uses an ACT 25 triode in a co-axial cavity driving an ACT 28 triode output stage also using a co-axial cavity. Both valves are anode modulated by pulses from a delay modulator using a 5C22 thyratron switch. The variable H.T. supply for the modulator is a voltage doubler using a 250 TH triode valve as the second rectifier. This valve is cut off during and immediately after the output pulse by a signal derived from the output pulse.

Reliability has been generally very good; the output power was increased appreciably above the original level by improving the match between the oscillator/driver and output valves and by altering the delay line impedance. The impedance change used existing components with a consequent reduction in pulse length of 1.2 ms; a line of correct length and impedance is to be provided.

Extraction Unit - a pulsed positive polarity supply; output variable from 1 to 25 kV; pulse length variable from 50 μs to 2 ms; 2 pulses/s maximum. Maximum output pulse current is 250 mA. Stability during the pulse is better than 0.25% at maximum loading.

The circuit uses a series selected CV2416 valve as the main element in a feedback loop operating only during the pulse period, the reference voltage and feedback amplifier being at the output potential. The series CV2416 valve also acts as a pulse switch using a CRT-photomultiplier light link for isolation from local ground.

During initial commissioning considerable trouble was experienced with pick-up from the r.f. unit causing incorrect output pulses. This was eventually solved by the use of clipping and limiting circuits in the light link switching circuit and by fitting a photo-multiplier valve combination in place of the photo-transistor/transistor circuit. A replacement/spare unit is being developed using similar principles but with two 4PR250C valves. One serves as the series control element; the other acts from ground as the output valve of the feedback amplifier/switch circuits, dispensing with the need for a light link and enabling reference and amplifier circuits to be at local ground level.

Gas Unit - provides a variable 2000 c/s continuous supply to the nickel leak controlling the hydrogen input to the ion source. Maximum output is 20 V r.m.s.,

normal working being some 6 V r.m.s., 4 A; the supply is not specifically stabilised.

P.I.G. Unit - functions so as to switch off all other platform units if the pressure in the column, as monitored by an ion gauge head on the ion column, exceeds a pre-determined level (normally 5 x 10^{-5} torr).

The gas unit and the PIG unit are housed in the same chassis and the units are similar to those previously used at the Laboratory on the 50 MeV proton linear accelerator. They have been completely reliable.

Light Receiver/Transmitter Pulse Unit - Initially, a unit using a photo transistor with transistor amplifiers was installed; due to its sensitivity to r.f. radiation from the r.f. unit and to thermal variations it was replaced by a photo-multiplier/valve circuit. This circuit is currently being superseded by a more sophisticated photo-multiplier/transistor combination.

Initial trials of this latest unit have shown that to a lesser extent it is susceptible to the same defects. It is now being modified so that where possible only high level signals are used at the platform end of the link, lower level signal processing being done at ground level.

The 'temporary' valve circuit provides two outputs - a 20 V, 20 μs, trigger pulse for firing the r.f. unit modulator and a 20 V pulse for gating the extraction unit output pulse. The relative timing of these two pulses is variable at ground level.

The system now being installed will provide the following facilities:-

Ground to Platform - two channels (one standby) for transmission of r.f. unit trigger and extraction unit gate (20 μs to 2.5 ms) pulses; relative timing and duration of extraction gate pulse is variable in the control room. A facility is provided for control of two extraction pulses (pilot and short) for use in injection studies. A current modulated light discharge source is used as transmitter and a photo-multiplier as receiver. Overall timing jitter is 0.1 μs.

Platform to Ground - for monitoring purposes, two channels are available for transmission of voltage pulses from platform equipment to the control room; pulse widths of 2 μs to 2 ms and amplitudes of ±100 mV to ±10 V can be handled, a standard amplitude calibrating pulse is fed in separately. Light transmission and reception is similar to that above.

High Voltage Focus Units - Output is continuously variable from 20 to 125 kV negative to local earth; maximum mean current is 300 μA; maximum pulsed current loading is 150 mA, 2 ms pulses. The stability of output during pulses is ±0.25% against input and output variations.

There are two identical units of this type using electrostatic generators. The stabilisation and control systems are similar to those of the 650 kV set. The charging resistor is 7 MΩ, storage condenser 25 nF and discharge limiting resistor 5 KΩ. Fast correction is to the earthy terminal of the condenser, the normally negative going signal being obtained from the anode of a 4PR60A valve.

Initially, the multi-stage rectifier sub-unit, which provides excitation for the electrostatic generator, proved unreliable in its 2000 c/s version. It was redesigned and has since given no trouble.

R.F. pick-up also caused appreciable variation of the output voltage during the pulse. This was cured by fitting an r.f. by-pass condenser directly from grid to cathode of the first stage of the feedback amplifier. Some failures have occured in inter-electrode insulation on the 4PR60A valves and also with one particular relay.

Low Voltage Focus Unit - A temporary unit was originally installed to determine the requirements for a final supply; this unit is still in use and is an unstabilised negative supply variable up to 10 kV maximum.

At present there is no intention to replace it by a more refined stabilised unit as its behaviour has been satisfactory.

Keep-Alive R.F. Supply - This is situated adjacent to the ion source in the 'bun' on the end of the accelerator column. It is a twin tetrode oscillator giving a c.w. output of a few watts at a frequency of 70-80 Mc/s, coupling to the source via single turn loops around the source hydrogen feed pipe. Its function is to provide a low level continuous discharge to ensure reliable ionisation by the main r.f. pulse.

The unit has given no trouble.

3.4. Linac

3.4.1. Linac Design

The r.f. design of the linear accelerator cavity was strongly influenced by the requirement that the drift tubes, of the Alvarez structure, should contain quadrupole magnets. R.F. defocusing forces dependent on operating frequency, acceleration rate and accepted beam radius, were balanced against the maximum attainable field gradient of a practical quadrupole that can be contained within a drift tube shell. On this basis, the minimum diameter for the drift tubes and the operating frequency, for a given acceleration rate, were determined. Also, in order to utilise the maximum axial length for each quadrupole magnet, drift tubes of a squarish cross section and small gaps between drift tubes, were desirable features.

Published data on re-entrant unit cell cavities (9) supplemented by some exploratory model cavity measurements, was used as the basis for the r.f. design. The chosen system employs constant drift tube and constant cavity diameters with the resonant frequency maintained by an increasing gap to unit cell length ratio. A useful reduction in this ratio at the high energy end of the linac is achieved by allowing a smooth change in the drift tube profile radius along the machine.

The final resonant dimensions were determined by precision model cavity measurements at a model frequency of 1000 Mc/s. (10). The resonant dimensional data was reduced to an algebraic form in which all dimensions were expressed as functions of unit cell length, such that it could be used in the computer programme which computed axial field distributions and the synchronous particle motion (3).

Some of the main r.f. parameters are given in Table 3.4.1(I)

TABLE 3.4.1(I): LINAC CAVITY PARAMETERS

Input energy	600 keV
Output energy	14.9 MeV
Resonant Frequency	115 Mc/s
Cavity length	13.45 m
Cavity diameter (nominal)	1.6945 m
Number of unit cells	49
Drift tube diameter	28.15 cm
D.T. profile radius	3.660 to 6.579 cm
D.T. aperture diameter	2.106 to 4.948 cm
Aperture profile radius	1.27 cm
Unit cell length	9.638 to 45.527 cm
Gap length	1.868 to 13.311 cm
Support stem diameter	4.445 cm
Theoretical Q factor	108,000
Measured Q factor	80,000
Calculated power required for 30° synchronous phase angle at the measured Q	802 kW
Frequency tuner range	± 23 kc/s
Flattener tuner range	± 300 kc/s
End to end field tilt range of tilt tuners	± 20%

3.4.2. Linac Construction

The linac cavity is fabricated from $\frac{1}{8}$ in thick rolled and welded copper sheet, riveted to a stainless steel framework of rings and longitudinal members. It is supported by four legs on the base of a separate mild steel vacuum vessel. Fig. 3.4.2(i) is a view of the linac with the vacuum vessel raised.

Tuning plates are situated in rectangular cut-outs in the cavity wall and are connected to the wall by convoluted flexible copper foil. There are four such frequency tuners which can be operated by push rods passing through the vacuum vessel. Two similar tuning plates are positioned one at each end of the cavity and are used for producing a tilt in the field gradient along the cavity. Two flattener tuners are used to correct for manufacturing errors in the resonant dimensions. Each of these is a continuous convoluted flexible plate, running from end to end of the cavity, with the longitudinal edges soldered to the inside surface of the cavity wall. They can be distorted locally by movement of a number of backing plates.

Two large rectangular cut-outs in the cavity wall form hatches for access to the inside of the cavity which can be blanked off by cover plates using garter spring r.f. joints to the cavity. There are some 350 uniformly distributed $\frac{3}{4}$ in by 5 in pumping slots in the cavity wall and 24 longitudinal water pipes are soldered to the wall to provide cooling and temperature stabilisation.

Each drift tube shell is constructed from a pair of machined copper spinnings, joined by a circumferential weld, with an axial tube, which forms the aperture, soft soldered in position at each end. The shell is located on the quadrupole magnet, which in turn is supported by a horizontal and a vertical stem. The end fittings of the stems are carried on the cavity framework and designed to allow alignment of the drift tube in all degrees of freedom. The support stems are sheathed with thin copper tubes, soft soldered into the drift tube shell, and r.f. contact is made between them and the cavity wall via flexible gaters and garter spring joints. A rough vacuum is maintained in the drift tube shells by pumping on the vertical stem. This stem also carries shell water cooling pipes. The horizontal stem carries the quadrupole conductor pipes. The arrangement can be seen in Fig. 3.4.2(ii).

3.4.3. Installation and Operational Experience

Drift tube alignment

The use of quadrupole strong focusing for the linac demanded very accurate alignment of drift tubes on to the axis. This alignment was carried out using a telescope, mounted from the cavity output end face, which could be set on to the line of sight between targets in the input and output end half drift tubes. Alignment was then by viewing targets in the input and output end of each drift tube bore. The targets were of metal having spark eroded V forms to which the telescope cross hairs could be set. A separate target plug was required for each drift tube because of their varying bore diameters. Alignment of the ends of each drift tube was to ±0.003 in in each plane and the mean of the measured misalignments of the two ends was less than ±0.002 in in each plane. The misalignment between magnetic and mechanical axes was previously determined and allowed for in the alignment process. (Errors due to all other sources were estimated to be less than ±0.002 in).

Longitudinal positioning of drift tubes was carried out using a telescope set up on a line of sight external to the cavity and parallel to its axis. This telescope was fitted with a 45° prism so that it could view drift tube faces through appropriate pumping slots, and was mounted on special rails running the length of the cavity. Distances from the input end face of the cavity were measured by referring the telescope position to a calibrated stainless steel tape. With corrections being applied for manufacturing errors in drift tube lengths and for the tolerance error in the overall cavity length allowed in manufacture, the accuracy of drift tube positioning varied between ±0.002 in at the input end to ±0.004 in at the output end of the linac.

Field Flattening

The distribution of axial electric field along the length of the cavity was measured by the frequency perturbation technique. The linac was designed to operate with a flat field, that is, all sections of the cavity tuned to the same resonant frequency to give gap voltages directly proportional to unit cell lengths. Since

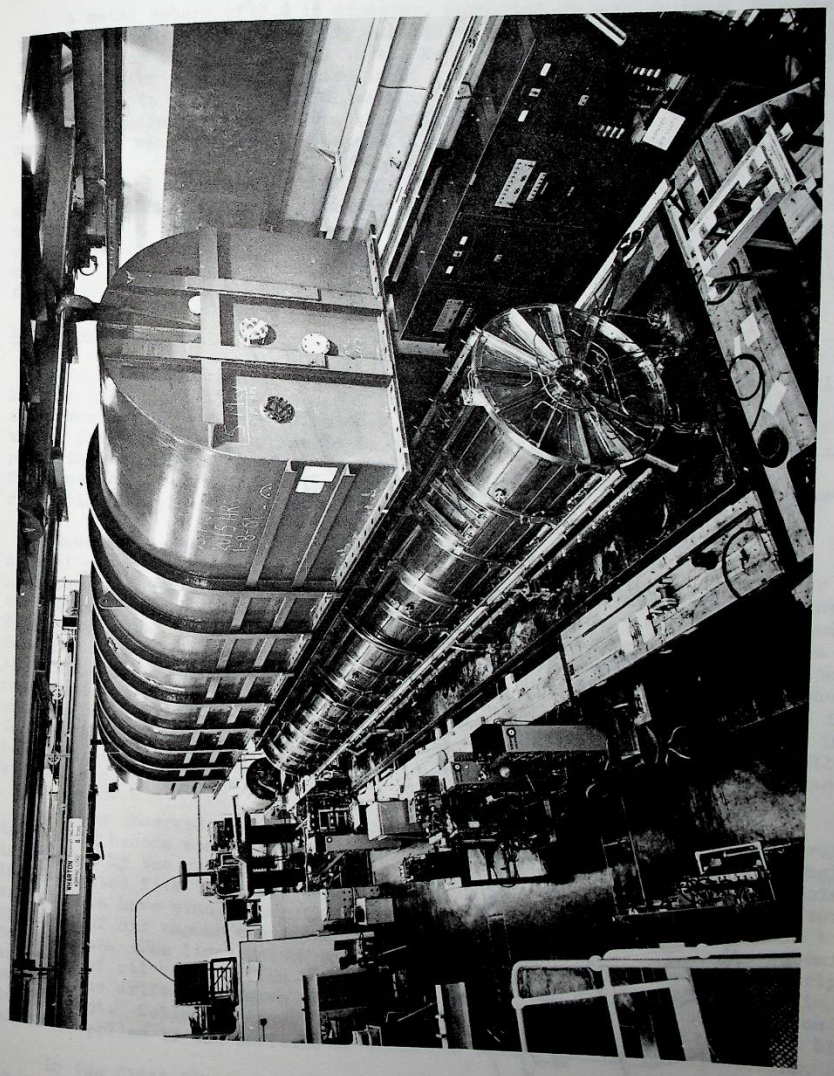

Fig. 3.4.2(i) View of the Linac with the Vacuum Lid raised.

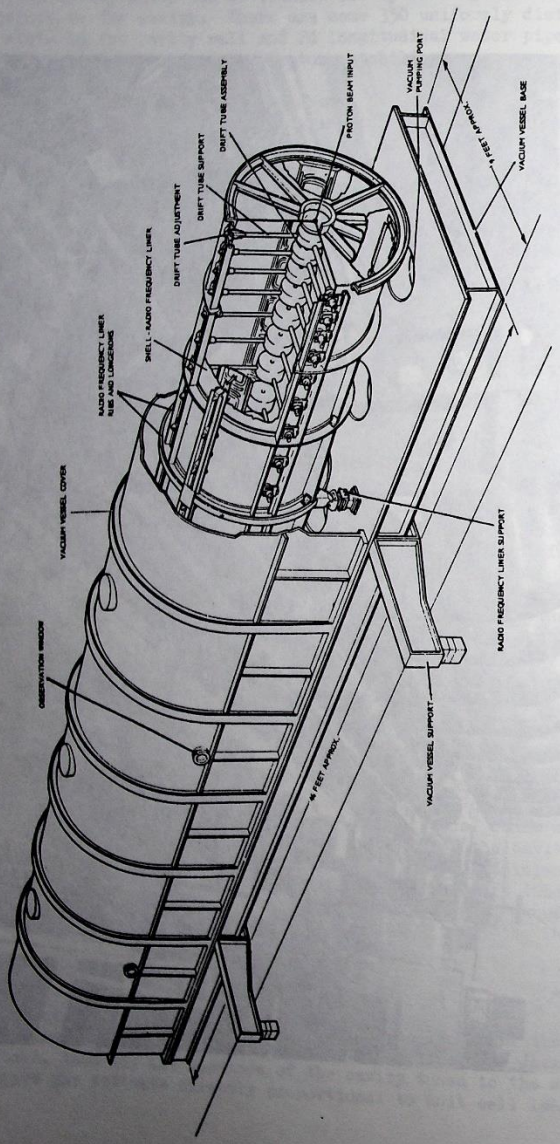

Fig. 3.4.2(ii) Cutaway view of Linac.

the field distribution across each gap was known the mid-gap fields only had to be measured.

A metal sphere of 0.4 in diameter, supported on a nylon cord, was used as the perturbing body, with the cavity excited by a lock-in oscillator. Frequency perturbations of about 100 c/s in 115 Mc/s were measured by a digital frequency meter. In the short gaps at the input end of the linac the sphere was too large in relation to the curvature of the field, and measurements were taken with a sphere placed off axis between the flat faces of the drift tubes. The two methods of measurement were overlapped at a suitable point along the cavity.

The axial electric field was related to the magnet field at the cavity wall, also measured by frequency perturbation using a flat metal plate placed through pumping slots, and in the final stages of the field flattening procedure it was only necessary to measure this magnetic field distribution. The electrical length of the cavity is comparatively short and it was an easy matter to adjust the flattener tuners to give a field flatness of ±1%.

R.F. Operation

The first attempt to feed the linac with high r.f. power was made on 1st July 1961 and the first 15 MeV beam was produced on 1st August 1961. Operation in the early months was severely affected by multipactor discharges, the effect of which was to prevent the cavity fields from rising above a very low level. Multipactoring usually occurred on over 20% of all pulses at a pulse repetition frequency of 1 pulse/8s, and the multipactor rate rose sharply as the pulse repetition frequency was increased.

Several methods to overcome multipactoring were tried in addition to careful cleaning of all drift tube surfaces. It has been observed on other machines that the drift tube surfaces become conditioned against multipactoring as the machine is run for a period of time. Accordingly the linac was operated at different pulse rates and under various conditions for long periods, but no tendency to condition was observed. Also, the rate of rise of r.f. drive power to the final amplifier was increased greatly in an attempt to drive through the multipactor level as rapidly as possible. The rise time of the r.f. field in the anode circuit of the final amplifier was reduced to as low as 2 μs without improving the multipactor breakthrough rate. It is believed that this particular failure may be explained by the existence of a glow discharge, seen at the r.f. feed vacuum window, providing a copious supply of primary electrons.

It was observed that, after only a few hours of multipactoring, the drift tube faces became coated with visible films, the pattern formed being strongly influenced by the quadrupole fringe fields. The secondary emission coefficient of the deposited film therefore determined subsequent multipactoring. Laboratory experiments have since shown that bombardment of a surface by electrons in the presence of oil vapour can produce a carbonised film with a low secondary emission coefficient. The linac vacuum system, however, is thought to be particularly clean and free of oil vapour. The next approach was to provide an artificial film by coating the drift tube faces with a material of known low secondary emission coefficient. Colloidal graphite was unsuccessful, but a mixture of carbon black in alcohol applied to the surfaces by brush has eliminated the multipactoring.

In the first instance all drift tubes were coated in this way with the result that the short gaps at the input of the linac required many hours of spark

conditioning. There was also a considerable increase in X-ray production at high field levels. Subsequently these short gaps have been cleaned of carbon black without reintroduction of multipactoring. As time permits the effect of cleaning off further gaps will be tried, as it is believed that field emission of electrons from these surfaces is a significant source of r.f. power loss.

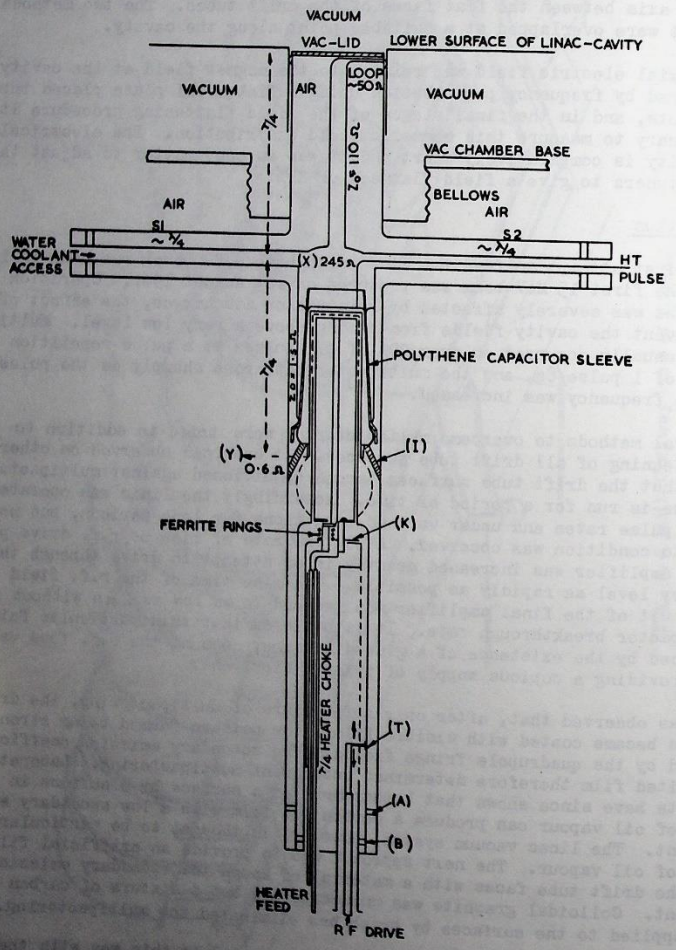

Fig. 3.4.4(i) Schematic Diagram of the RS 1041 Valve Circuit.

3.4.4. Linac R.F. Drive System

Design of Valve Circuit

The system was required to provide r.f. power of 1.5 MW in pulses of 2.5 ms at a repetition rate of up to 2 pulses/s maximum. Provision of this level of power at a frequency of 115 Mc/s, presented the problem of finding a valve (or valves) with suitable geometry, and a cathode equal to the unusually long pulse duration. The original intention, to use six E.E.Co type BW165 in some parallel - push pull arrangement, was abandoned when the use of one Siemens' type RS1041 was confidently advocated by the Siemens Labs.

This valve, designed for 30 Mc/s operation, has a geometry far from ideal for operation at 115 Mc/s in a co-axial type circuit, but its ability to meet the long pulse requirement made the circuit design a worth-while undertaking.

At the outset a decision was taken to couple the anode-circuit of the valve direct to a loop in the linac-cavity via an impedance transformer, and thus avoid the use of a matched coupling line with possible problems of breakdown during the mis-matched 'build-up' period in the cavity. This decision was the result of experience with a type BW165 valve, driving a cavity approximately equivalent to 2 unit cells of the linac. The r.f. arrangement used in this experiment differed considerably from the system designed for the RS1041, but the common factor was the use of direct coupling to the loop via an impedance transformer. The experimental rig performed satisfactorily both as a driven system and as a single valve self-oscillator, producing about 45 kW r.f. in the cavity. A further decision to isolate the anode system and cavity loop from the vacuum system, by the use of an insulating lid, determined in some degree the basic layout of the RS1041 circuit.

Figure 3.4.4(i) shows the circuit in schematic form approximately to scale. The considerable length of the RS1041 elements in relation to the external circuits has a major effect on the external circuit dimensions. This coupled with the design decisions mentioned, had to be arranged to provide impedance transformation from anode to cavity feed-loop, and tuning for resonance of grid-cathode circuit with impedance matching of drive-power input-line.

Anode-Grid Circuit - An anode impedance of ~ 210 Ω required matching to a loop impedance arbitrarily fixed at 50 Ω . The 210 Ω is, however, transformed by the long conductors within the valve to the low value of ~ 0.6 Ω at the output seal, (plus a reactive component which can be tuned out by the outer piston, (A)).

Direct transformation of 0.6 Ω to 50 Ω by a single quarter-wave section was not possible for various structural reasons, a minimum length of half-wave being unavoidable. The diameter of the valve anode with water-cooling jacket, and the necessary anode-blocking capacitor formed around it, dictated the minimum inner-conductor diameter for the first quarter wave section. Since the end of this section (point X) would be a voltage anti-node the impedance was kept to a value where the peak-voltage would be unlikely to cause troublesome sparking, particularly during mismatch conditions. Allowing some license in considering the geometry around the support insulator (I), the section (Y)-(X) is presumed to have a Z_o of 12 Ω making the impedance at (X) ~ 245 Ω . From this point it was a simple matter to provide a 110 Ω

3.4.5. Drive Chain

About 140 kW r.f. power is required to drive the RS1041, in class 'B' operation, to an output of 1.5 MW. The 'drive-chain' amplifies from crystal-oscillator level to 140 kW in a total of 10 stages, the first four low-power stages being used for frequency multiplication from the crystal frequency of 106.481 Kc/s.

The oscillator and a x 10 stage have a short-term stability of ~1 or 2 in 10^8 and a long-term of 1 in 10^7. The three further stages of multiplication are x 6, x 3 to 115 Mc/s at an output power of ~3 W c.w.

The remaining five amplifiers are pulsed and are all constructed to a similar r.f. design - a half-wave co-axial anode-line tuned at its open end by a polythene slug, with the HT pulse fed in at the voltage node, and the r.f. output taken via a loop in the same region. The grid is grounded, r.f. drive being applied to the heater-cathode element, a suitable input impedance being provided by chokes in the supply-leads.

This chain of five uses valves in the order:-

3W → ACT.25 (x 10) → ACT.25 (x 10) → ACT.27 (x 6) → BR1106 (x 10) → BW165 (x 8) → 144 kW

R.F. output from the BW165 is fed to the cathode circuit of the RS1041 via a stub-supported '3 inch' 50 Ω co-axial line.

3.4.6. Modulators

Two modulators are used, one to operate the five drive-stages via a suitably tapped pulse-transformer, and a 'main' modulator to supply the RS1041. A tapping on this modulator is also provided to power the BW165 driver, if required.

The main modulator - provides an output pulse to the following specifications:-

Pulse Voltage	30 kV (Tapping at 22.5 kV)
Pulse Current	85 A
Pulse Length	2.5 ms
Pulse Recurrence	2 pulses/s
Pulse Rise-time	100-200 μs
Pulse Voltage Stability	±0.5% pulse to pulse
Pulse Voltage drop	0.5% max. into resistive load

These requirements have been very closely met, and except for a few minor faults the modulator has behaved very well.

The drive-chain modulator - is mainly of laboratory manufacture, it is rated at 500 kW. The pulse-network voltage is stabilised to 0.5%. The output pulses are at the levels 1 kV, 2 kV, 5 kV, 8 kV, 22.5 kV and have substantially flat tops.

3.4.7. R.F. Commissioning

No measurement of high-level power output from the RS1041 was made prior to the circuit being assembled in position under the linac. Coupling to a dummy-load

in the absence of the usual anode resonant-circuit and matched out-put line presented a number of difficulties. Tapering from the 12 in dia. co-ax at the loop, to a smaller diameter transmission line and a dummy load could have been constructed, but was not considered justified in view of cost and time-scale. Various disc-shaped loads were tried in place of the 50 Ω loop and powers up to 500 kW were measured in this way, always limited by tracking breakdown or excessive current density at the centre connection.

After installation under the linac, the system was run-up in air until drift-tube breakdown occurred. When everything was optimised this level was reached with a 6 kV pulse to the RS1041, corresponding to about 50 kW in the resonator, if an anode-efficiency of 60% is assumed.

Operation with the linac evacuated, does not affect the drive circuitry except for a slight change of frequency which is well within the bandwidth of the circuits. Once the 'multipactor' effects were eradicated attention was given to the operation of the system under self-oscillatory conditions.

It was known that some system would need to be evolved eventually, to allow for the high reactive loading of the cavity by the high current beams ultimately expected. Automatic control of the source frequency during the pulse was a possibility, but a self-oscillatory system with the resonator the sole frequency determinant was more attractive on the grounds of simplicity.

Such a system has been in operation during most of 1962, and apart from the anode-capacitor troubles mentioned earlier the system is apparently reliable and simple.

Only the two final valves in the chain are used, the BW165 driver and the RS1041. Drive for the cathode of the BW165 is taken from a small loop in the linac resonator. The co-axial line conveying the drive includes a half wave 'line-stretcher' which is adjusted to produce the correct over all phase-relationship for positive feed-back. If necessary a further 180° can be obtained by reversing any coupling loop in the system.

Operation with only two valves, further simplifies matters by eliminating the need for two modulators. The tapping on the 'main' modulator provides pulse power for the one drive-stage.

The acceleration of beams over 3-4 mA places sufficient loading on the resonator to necessitate some arrangement of r.f. power level stabilisation for constant accelerating field.

A simple feed-back arrangement has been in use for some weeks, giving good power level correction during the beam pulse. Advantage was taken of the wide variation of r.f. level in the linac-resonator, obtainable merely by variation of the BW165 H.T. pulse. By feeding the BW165 H.T. via 600 Ω and shunting the valve with one of adequate power capabilities (BR1106), the field level in the linac can be controlled by control of the shunt valve grid-voltage. To complete the feed-back link, some r.f. from the linac cavity is taken via a loop to a diode rectifier and thence to a diode 'gate'. Here the unwanted portion of the pulse is 'clipped' off leaving just the top with its 'loading' signal to be passed on through amplifiers to the grid of the shunt valve, BR1106. The sign of the feed-back is such that a fall in field-level is transmitted to the BR1106 grid as a negative signal, thus

allowing the BW165 H.T. voltage to rise giving increased drive to the RS1041 and higher power in the linac cavity.

A range of approximately 2:1 in power-level will need to be controlled by this device if an accelerated beam of 50 mA is realised.

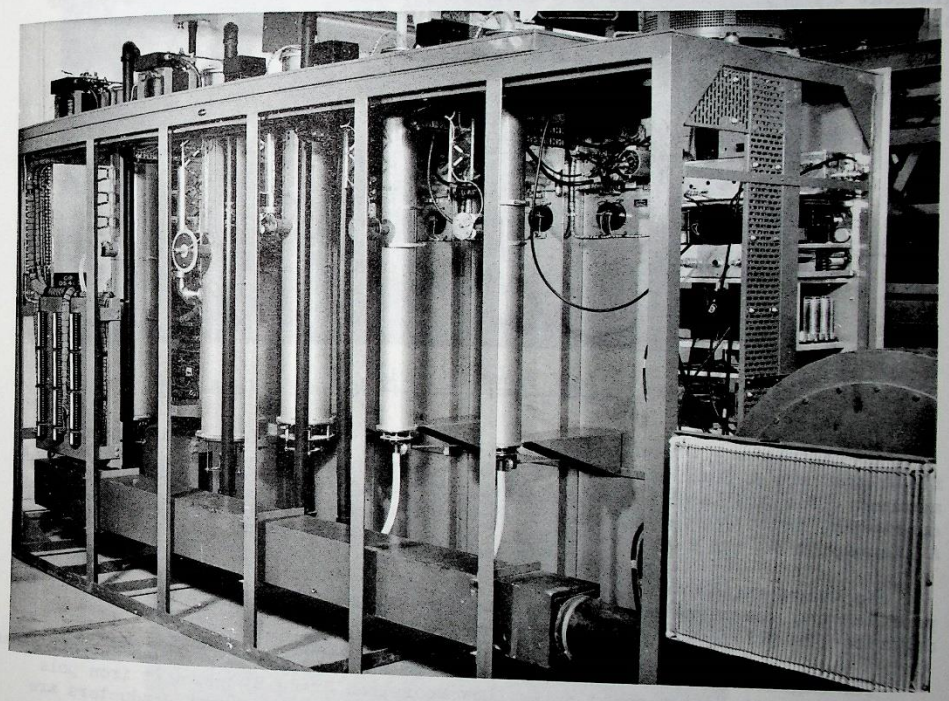

Fig. 3.4.5(i) Rear view of RF Drive Chain Cubicles.

3.4.8. Linac Quadrupoles

(a) Basic design parameters and construction

The quadrupoles, which form part of the linac drift-tube assemblies, were designed to provide a constant focusing or defocusing impulse per half focusing period, along the length of the linac. This means that the effective strength of the quadrupoles follows the law $A_{eff} \propto \beta^{-1}$, where A_{eff} is the effective field gradient and β is v/c (v- proton velocity). The linac unit cell considered for the calculations was as shown in Fig. 3.4.8(i).

Fig. 3.4.8(i) Linac Unit Cell

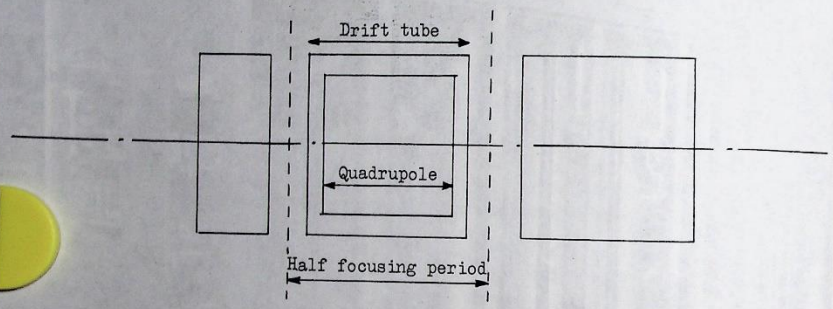

In calculating the effective strength of the quadrupole A_{eff} in terms of the field gradient A_0 inside the magnet, hard edged magnets (no fringe fields) were assumed. The gradient of the input quadrupole magnet (and hence drift-tube) apertures, input energy and linac r.f. frequency are all closely interdependant. A discussion on the selection of these parameters appears in (1).

No calculations or detailed experiments were performed on the pole tip profiles and the results of other workers were used. The magnet calculations are described in (11), (12) and (13).

The magnets consist of a mild steel yoke to which the drift-tube support stems are welded, soft iron tapered poles (Low Moor Iron Grade B) and soft iron pole tips (Low Moor Super Hiperm). Hollow, low-voltage, high-current conductors are used for the quadrupole windings. These are wound with a number of cross-overs between poles to eliminate unequal heating effects on the poles and to provide a symmetrical array of conductors at the ends of the magnets. The ratio of conductor inner to outer diameters was chosen to give the minimum temperature rise of the magnet cooling water. Each magnet winding was formed from a continuous length of vacuum-tested tube, the conductors entering and leaving the drift-tube via the horizontal support arm. A combined high-pressure water (100 lb/in^2) and high current (500 A) coupling is used at the end of each conductor emerging from the drift-tube stem. There have been no vacuum or electrical troubles at this junction.

Extensive use is made of epoxy resin-bonded fibreglass for insulation between the magnet windings and the poles and between winding turns. Steatite sleeves are used for insulation at the junction of the stem to the yoke (to allow an argon-arc

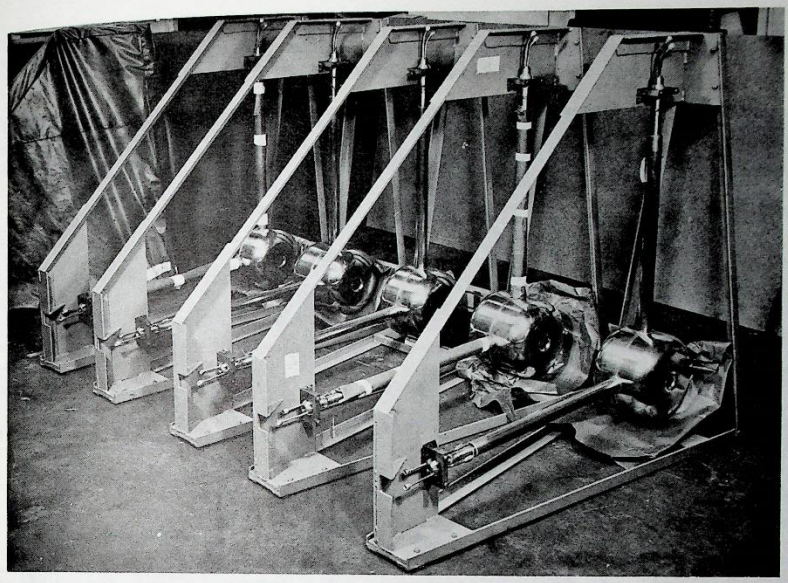

Fig. 3.4.8(ii) Linac Drift Tubes in Transportation Frames.

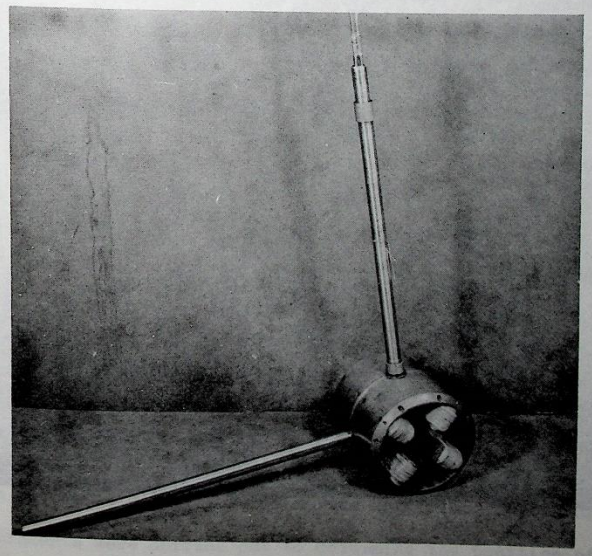

Fig. 3.4.8(iii) Linac Drift Tube showing Quadrupole Magnet.

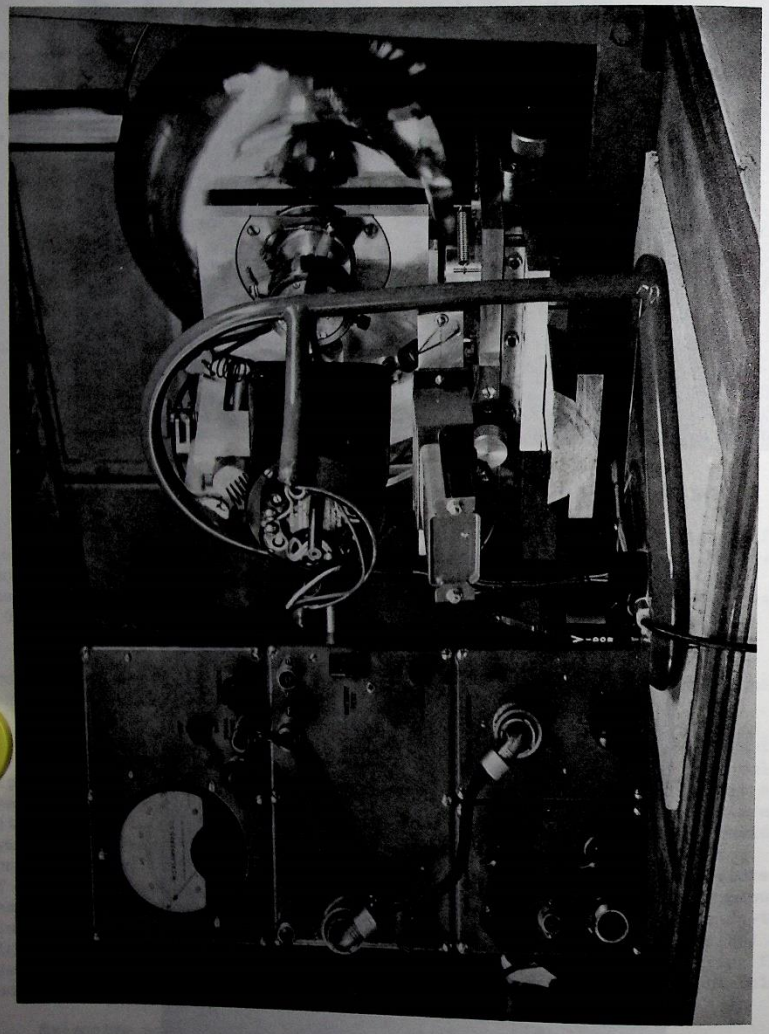

Fig. 3.4.8(iv) Magnetometer used in measurements at the Laboratory.

weld to be made after part assembly of the quadrupole). Insulation inside the drift-tube stem is provided by woven glass sleeving. The two conductors leave the stem via a combined vacuum joint, made of a split neoprene bung.

Insulation resistance to frame in excess of 100 M Ω (500 V Megger test) was measured for all drift-tubes after trouble from "conducting" neoprene (heavily loaded with lampblack) had been eliminated. No vacuum troubles have been experienced at this point.

(b) Magnetic Measurements and Testing

A comprehensive series of mechanical, electrical and magnetic tests was carried out on each quadrupole prior to welding on the drift-tube spinnings. These tests were carried out at the manufacturer's. A further series of measurements was carried out at the Rutherford Laboratory after delivery of the completed drift-tube assemblies. (The magnetometer used in these measurements is shown in Fig. 3.4.8(iv)).

(i) Sub-assembly tests at the manufacturer's.

Mechanical checks – correct orientation of winding pre-form and yoke; condition of pole tip surfaces, etc.

Electrical checks – measurement of d.c. resistance.

– measurement of A_o(gradient)/I(current).

– checks for shorted turns : two rejects.

– insulation winding/frame : three rejects.

Magnetic checks – position of magnetic axis relative to pole tips : one reject (shorted turns).

– orientation of transverse zero potential planes relative to drift-tube stems.

Every case of failure was investigated fully and corrections made at the source of the trouble. The acceptance limits for these magnetic and electrical tests were as follows:-

Insulation	$\not<$	10 M Ω (500 V Megger test)
Magnetic Axis	$\not>$	0.002 in from centre of best tangent circle to the four pole tips.
Transverse planes	$\not>$	0.25° from correct position (as defined by scratch marks on yoke).

The magnetic tests were based on rotating coil techniques and the magnetometers used were developed specially for the purpose.

(ii) Tests on completed drift-tubes at the Rutherford Laboratory.

Measurements were carried out to determine the position of the magnetic

axis at each end of every drift-tube relative to the optical axis as defined by alignment targets placed in the drift-tube bore. The final optical alignment of the drift tubes in the linac made use of the corrections obtained in these tests. (Due to the method of construction of the drift-tubes, the central tube may not be perfectly aligned with the quadrupole.)

Another specially developed rotating-coil magnetometer was used and the measurement accuracy was estimated to be better than 0.00025 in.

A final check of insulation resistance after drying of the quadrupole (by evacuating the drift-tubes) and after replacement of the neoprene bungs, showed resistances well in excess of 100 M Ω (500 V Megger) for every drift-tube magnet.

3.4.9. Quadrupole Power Supplies and Gradient Boxes

The linac quadrupoles are connected in six series groups, each group having a separate voltage stabilised transformer rectifier set with an LC filter. To enable different current distributions to be obtained along the length of the series connected chain of quadrupoles, difference currents are fed in or led off at the inter-magnet connections.

The purpose of the gradient boxes is to control the feed and bleed currents and allow two pre-set current distributions to be obtained by switch operation and control of supply voltage to the group of quadrupoles only. The two distributions concerned are those appropriate to:-

(i) Normal "High Law" - $A_{eff} \propto \beta^{-1}$ (as mentioned in 3.4.8(a))

(ii) "Low Law" - $A_{eff} \propto \beta^{-3/2}$

The networks for the gradient boxes (Fig. 3.4.9(i)) were calculated using the results of the d.c. resistance and the A_o/I measurements referred to in 3.4.8(b).

Voltage stabilisation supplies are used in preference to current stabilisation for the power supplies since this facilitates setting up the current distribution network and allows for individual control of the input half quadrupole and the output half quadrupole. The voltage sensing leads for the first and last groups do not include the input half quadrupole and the output half quadrupole. The resistance of the quadrupole windings is maintained constant by the use of temperature stabilised cooling water.

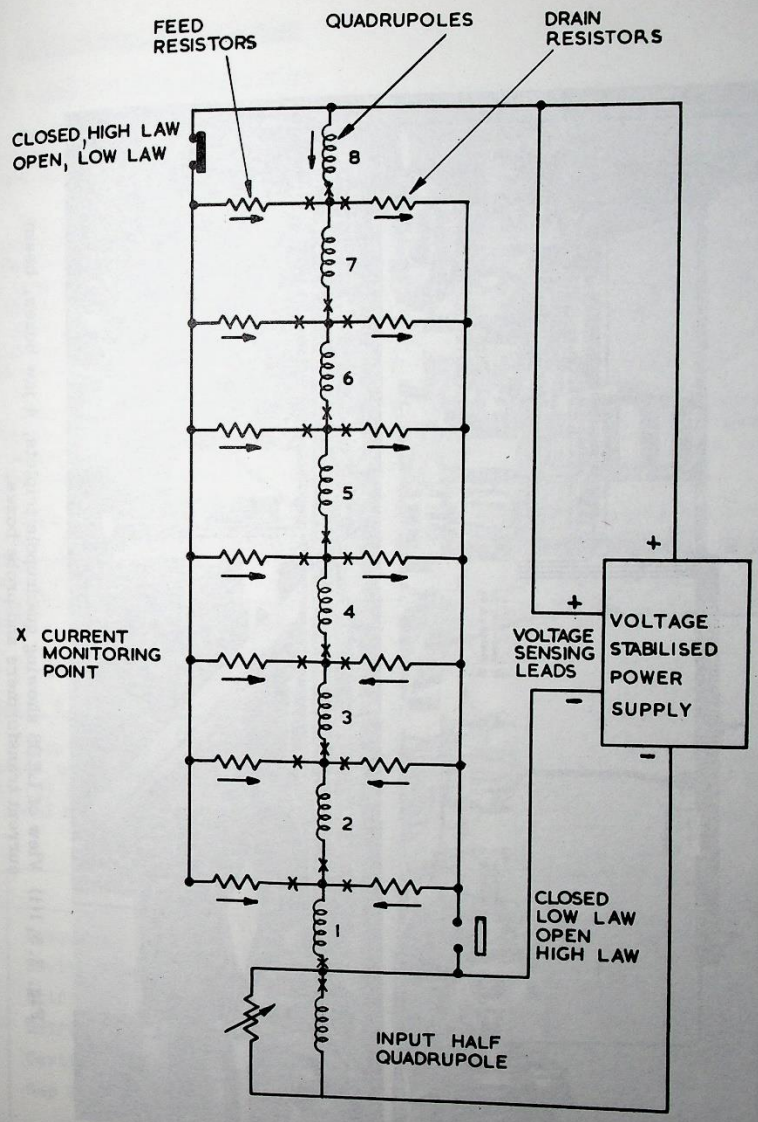

Fig. 3.4.9(i) Simplified Schematic Diagram of First Gradient Box.

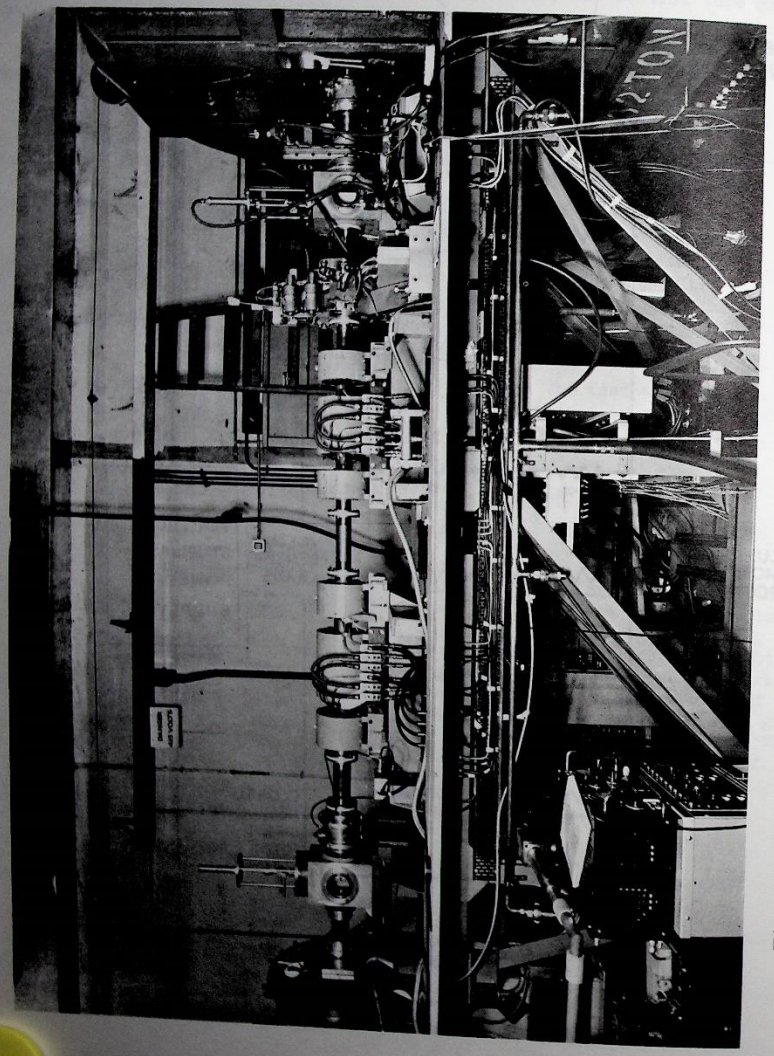

Fig. 3.5.1(i) View of LEDS showing quadrupole triplets, 4 jaw boxes, beam current transformers and probe boxes.

3.5. Drift Spaces and Inflector

3.5.1. LEDS and HEDS Quadrupoles

Quadrupole triplets are used in the low energy drift space (3 triplets) and the high energy drift space (4 triplets) for beam matching purposes. The required values of gradients and apertures were obtained by computation.

The quadrupole magnets were designed in the same way as for the linac quadrupoles (see 3.4.8) and are constructed in a very similar manner. The main differences between the linac quadrupoles and the beam matching quadrupoles are the larger apertures ($2\frac{1}{2}$ in, 3 in and $3\frac{1}{2}$ in diameter) and the smaller gradients of the latter. The beam matching quadrupoles have gradients in the LEDS of 100 to 200 gauss/cm and those in the HEDS of 300 to 400 gauss/cm. The magnetic circuit design is common to the quadrupoles in both drift spaces; the difference between quadrupoles of a particular aperture lies in the number of turns/pole.

Only electrical tests were conducted on the beam matching quadrupoles in view of their relative accessibility and the excellent agreement found between mechanical and magnetic axes with the quadrupoles for the linac. These involved investigation of the number of turns/pole, shorted turns and insulation to frame.

Each triplet is powered by a transformer rectifier set with an output LC filter. All three elements of the triplets are connected in series, with the outer elements adjacent to each other. This enables the outer elements to be shunted relative to the centre element or vice versa. Low resistance, wide-range, adjustable shunts, using transistors, are employed to give ±15% out-of balance control. A description of these shunts can be found in (14).

3.5.2. Buncher and Debuncher Cavities

General R.F. Design

Both buncher and debuncher are single gap cavities of re-entrant geometry, similar to a single unit cell of the linac. Their design was based on published data (9) and accurate resonant dimensions, given in Table 3.5.2(I) were determined by model measurements at 1000 Mc/s.

TABLE 3.5.2(I) BUNCHER AND DEBUNCHER PARAMETERS

	Buncher	Debuncher
Frequency	115 Mc/s	115 Mc/s
Cavity diameter	41.054 in	41.054 in
Drift tube diameter	11.084 in	11.084 in
Drift tube profile radius	2.590 in	2.590 in
Cavity length	11.309 in	25.774 in
Gap length	0.805 in (with grid)	3.290 in (no grid)
Drift tube aperture diameter	2.250 in (aperture through grid)	3.937 in

In the design of the buncher, a high value for the ratio of shunt impedance to Q-factor was sought because the buncher has an artificially loaded Q-factor to give good electrical stability. At the same time a short axial length for the buncher is required because of space restrictions in the LEDS.

The debuncher power requirement is such that it is not practical to reduce its Q-factor artificially and so a high value shunt impedance was chosen. For both cavities a reasonably small diameter was desirable. The theoretical figures for the power requirements are given in Table 3.5.2(II).

TABLE 3.5.2(II) BUNCHER AND DEBUNCHER THEORETICAL POWER REQUIREMENTS

	Buncher	Debuncher
Peak energy change of proton	21 keV	200 keV
Peak gap voltage	22.8 kV	230 kV
Q-factor (unloaded)	26,200	35,100
Q-factor (loaded)	920	-
Cavity r.f. dissipation	177 W	6,030 W
Total r.f. power required	5,040 W	6,030 W
Proton drift distance from the linac	1.44 m	10.7 m

Tuners

Adjustment of the gap length by moving one of the half drift tubes provides course tuning of each cavity. The r.f. connection of the adjustable half drift tube to the cavity end wall is by a convoluted copper diaphram. The buncher has two fine tuners, similar in design to those in the linac, one of which can be operated remotely. The debuncher has a single fine tuner which is servo-operated. The servo error signal is derived from the phase comparison of r.f. signals from the cavity and its feed line, in a coaxial cable rat-race phase bridge.

R.F. Feeds

Each cavity is fed with r.f. power from a pick-up loop coupled to the linac. This method of feeding the cavities is preferable to coupling from some point in the linac drive chain, since it ensures that the drive to each cavity maintains a constant phase relationship with the linac fields. The drive level can be adjusted by varying the pick-up loop penetration in the linac and similarly the feed loop to each cavity can be adjusted to give an r.f. match to the feed line. Phase adjustment is achieved by a line stretcher and the r.f. match can be monitored by a reflectometer.

Mechanical Construction

The debuncher cavity is similar in construction to the linac, being fabricated from copper sheet riveted to a framework of stainless steel ribs. The buncher is constructed from $\frac{3}{8}$ in copper plate, rolled and welded with internally machined

surfaces. The end faces are also of copper plate backed by stainless steel ribs.

Both cavities have separate vacuum envelopes; the debuncher has domed end walls but the buncher has flat end walls to minimize the overall length. Both are pumped with single 9 in mercury diffusion pumps.

Operation

Only the buncher cavity has been operated at high power. This cavity is suffering from multipactor troubles at the present time, in spite of the use of a d.c. bias. The bias, of up to 3 kV, is applied to one cavity end wall, which makes r.f. connection to the cylindrical wall through a capacitive joint insulated by 0.010 in polythene sheet.

One cause of the trouble may be r.f. field leakage from this joint into the cavity - vacuum vessel interspace. If the bias suppression of multipactor proves unsuccessful, the buncher surfaces will be coated with carbon black. The debuncher cavity, which is to be commissioned early in 1963, is also designed to have d.c. bias in the same manner.

3.5.3. Steering Magnets

Beam steering facilities are provided at the output end of the linac, (14), using four magnets (M_1 to M_4), and at the inflector using two magnets (M_5 and M_6).

The system consisting of M_1 to M_4 is designed to align any matched output beam from the linac with the theoretical beam line. The requirements of minimum axial length and momentum resolution are self consistent and consequently the system was designed to occupy not more than about 1 m of flight tube. The magnets M_1 and M_3 steer the beam vertically and M_2 and M_4 steer the beam horizontally.

The magnet design can be seen in Fig. 3.5.3(i) and the magnet parameters are given in Table 3.5.3(I).

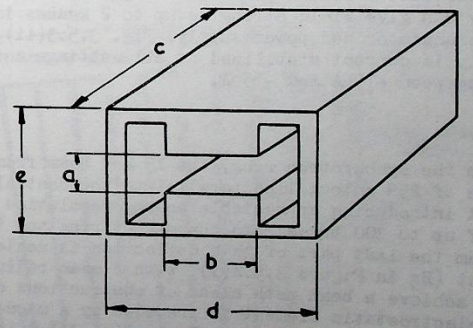

Fig. 3.5.3(i) Steering magnet design.

TABLE 3.5.3(I) STEERING MAGNET PARAMETERS

MAGNET / PARAMETER	M_1	M_2	M_3	M_4
Pole Separation: a (cm)	8	8	5	5
Pole Width: b (cm)	16	16	10	10
Pole Length: c (cm)	20	20	15	15
Magnet Width: d (cm)	40	40	25	25
Magnet Height: e (cm)	20	20	15	15
Ampere-Turns	8,210	6,850	6,360	6,140
Flux Density (kgauss)	1.29	1.075	1.6	1.54
Total Coil Area: (cm^2)	50.3	44.2	41.0	39.5
Power Consumption (W)	260	200	125	120
Approximate Weight (lb)	240	240	200	200

At the inflector, magnets M5 and M6 allow the beam to be steered vertically. Horizontal steering can be achieved at this point by means of remotely operable shunts on the first two sector magnets of the inflector.

The magnets are constructed from Super Hiperm Magnetic Iron which has a low remanent field and they can give field strengths up to 2 kgauss in either direction. A specially developed transistorised power supply, Fig. 3.5.3(ii), is used to power the magnets. The supply is current stabilised at all settings and is continuously variable through zero between +15 A and -15 A.

3.5.4. Inflector

For injection into the synchrotron ring, the 15 MeV beam from the linac must be turned through an angle of 25° onto a line parallel to the central equilibrium orbit (Fig. 3.5.4(i)) without introducing appreciable energy resolution (16). To permit continuous injection of up to 300 turns into the magnet ring and to avoid excessive loss of circulating beam the last part of this deflection is achieved by means of an electrostatic element (E_5 in Figure 3.5.4(i)) with a mean radius of 6 m and a field of 55 kV/cm. To achieve a beam path clear of obstructions on to the required injection radius, the electrostatic element is preceded by a magnet. A suitable magnet has been designed (16), and is shown as E_4 in Fig. 3.5.4(i).

In order to inject the beam using these last two elements, it is necessary to deflect the beam from the linac beam line through an angle of 11.5° towards the

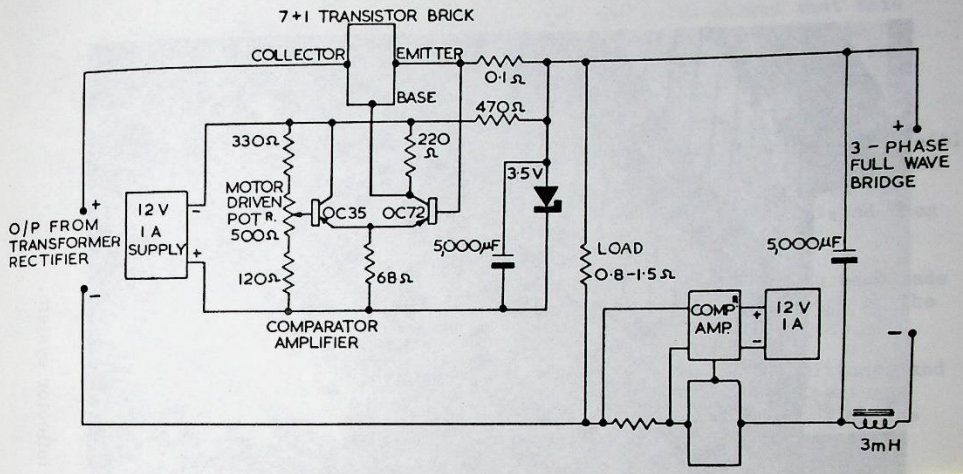

Fig. 3.5.3(ii) Steering magnet supply circuit.

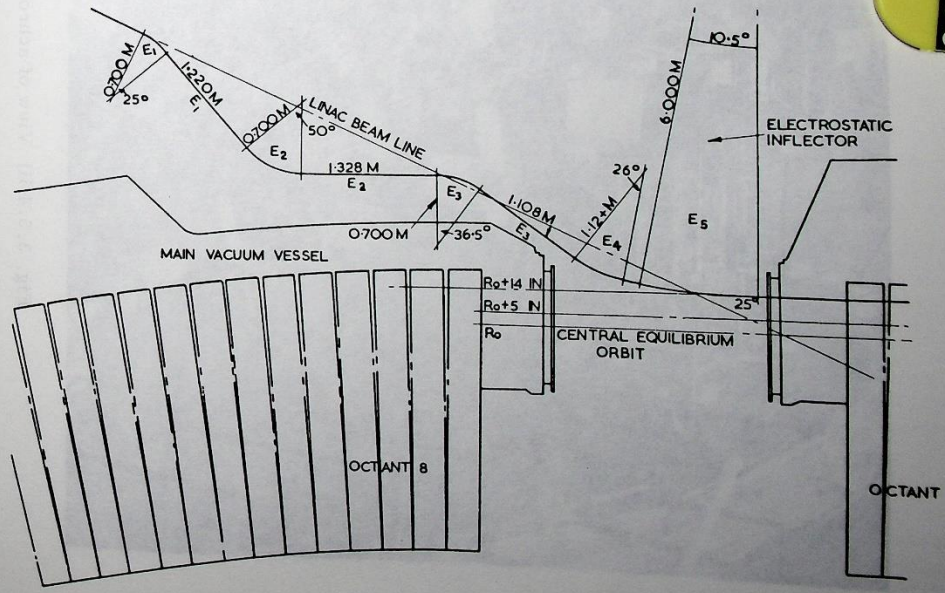

Fig. 3.5.4(i) Inflector

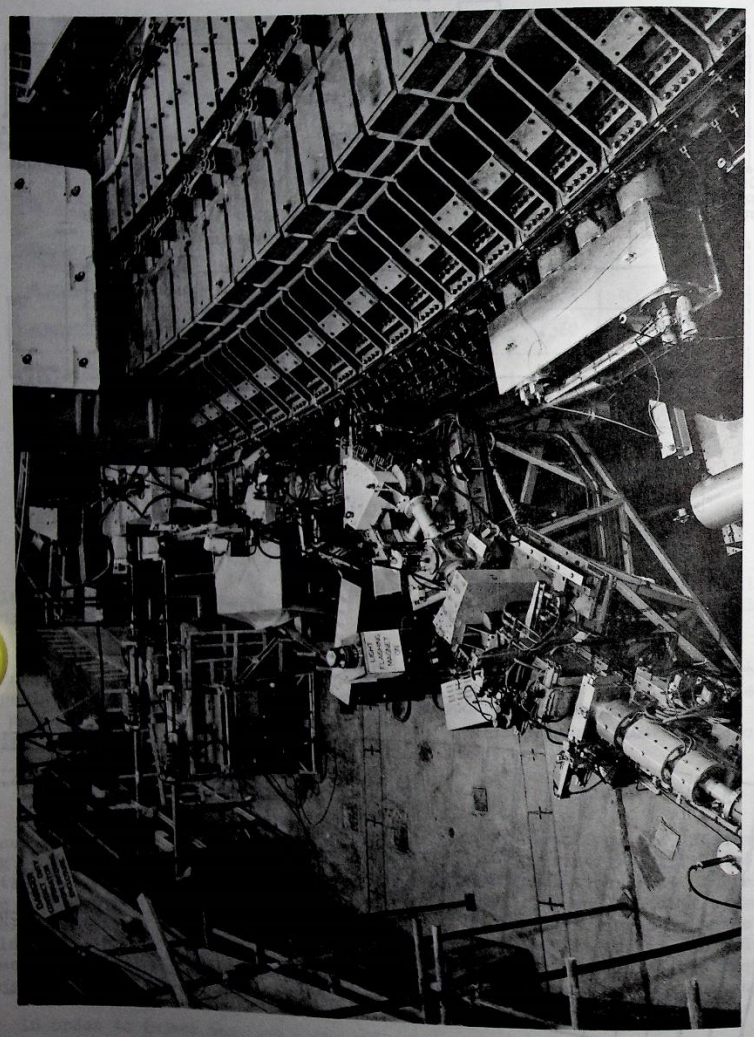

Fig. 3.5.4(ii) View of achromatic inflector system.

synchrotron. The simplest solution would be to produce this deflection by a single element but investigation of the resulting momentum resolution showed that this would result in an effective increase in emittance of about 48%. As this is not acceptable it was decided to design an achromatic system. This consists of four sector magnets followed by the electrostatic element.

The magnets E1, E2, E3 and E4 have apertures 9.25 cm vertically by 14 cm radially and have fields of 8, 8, 8 and 5 kgauss respectively. It was found possible to shim them to give $\int Bdl$ proportional to radius to within $\pm 0.02\%$ over a required good field aperture of 8 cm vertically by 4 cm radially. This was achieved by shimming first to give constant field in the central region of the magnet and then adding end shims to give an effective length proportional to radius.

Since the injection radius is not yet known precisely the system has been made adjustable so that the beam may be injected from any position from the edge of the good field region to up to 4 in inside the good field region.

Investigations of the focal properties of the system showed that emittance and momentum defining facilities could also be incorporated. The defining apertures provided will allow the definition of 'pencil' beams which can be used during the commissioning of the synchrotron and also of matched beams (17) during normal operation.

3.6. Other Injector Facilities

3.6.1. Beam Monitoring System

The beam pulse can be monitored at 12 points along the injector by means of toroidal beam current transformers (B.C.T.s) Any three of these may be selected and displayed simultaneously on a suitable oscilloscope either in the injector control room or in the main control room. The system is shown in Fig.3.6.1(i).

The beam intensity is measured by an amplitude reading which is compared with a current pulse (calibration pulse) of known, adjustable, amplitude which can be switched into any of the B.C.T.s.

The monitoring sequence is:-

B.C.T. → head amplifier → (balanced 100 Ω line) → selector box → calibration box (No. 1, 2 or 3) → oscilloscope.

(a) B.C.T.s

These consists of Selected Grade Mumetal ($\mu_o > 50,000$) cores 6.5 in o.d., 4.5 in i.d. x 1.5 in x 0.004 in. One type, for long pulses, is wound with 100 turns and a second type, with high sensitivity for short pulses, is wound with 10 turns. The turns are evenly distributed around the core, which also has 1 turn carrying the calibration pulse. Magnadur rings, diametrically magnetised and opposing each other are used each side of the current transformers for electron suppression. (Fig. 3.6.1(ii)).

(b) Head Amplifiers

These are situated near the respective current transformers and provide the necessary low load impedance for the transformers. They have low impedance outputs to feed 100Ω balanced cable to the injector control room and the main control room. The units are fully transistorised with two switched gain settings:-

Low gain, 1 mA input (100 mA beam current) → 10 V output across 100 Ω

High gain, 0.2 mA input (20 mA beam current) → 10 V output across 100 Ω

A self-contained battery operated version is available for "Faraday-Cup" monitoring with switched settings of 10 μA, 100 μA or 1 mA input, with an input impedance of 10 kΩ giving a 10 V output across 100 Ω .

(c) Selector Box

This is situated in the injector control room and contains uniselectors, for selection of transformers and routing of the calibration pulse and also has balance to unbalance pulse transformers. It provides manual control of transformer selection either in the injector control room, using calibration box No.1 or 2, or in the main control room using calibration box No.3.

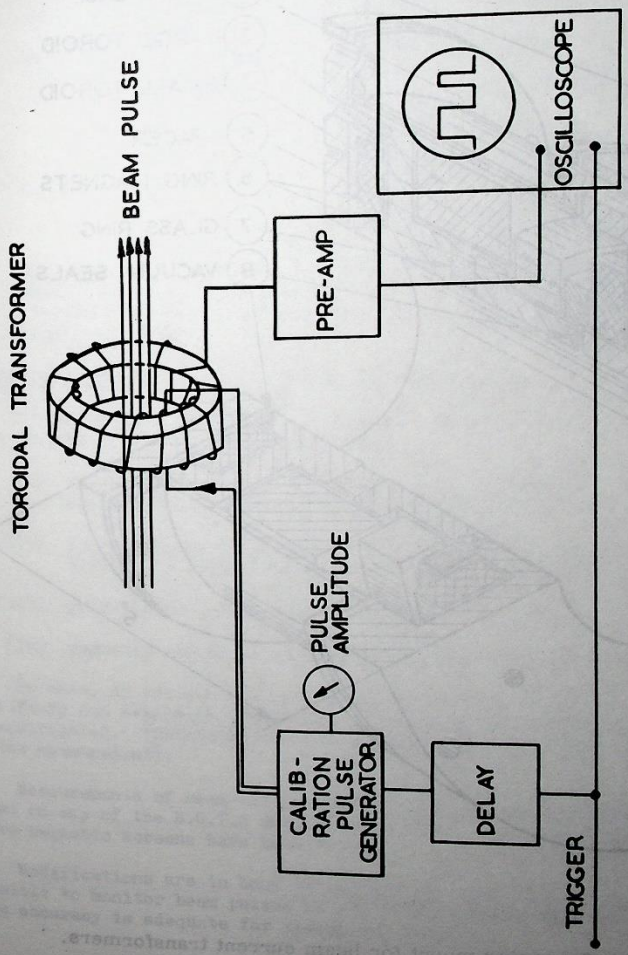

Fig. 3.6.1(i) Rudimentary beam monitoring system.

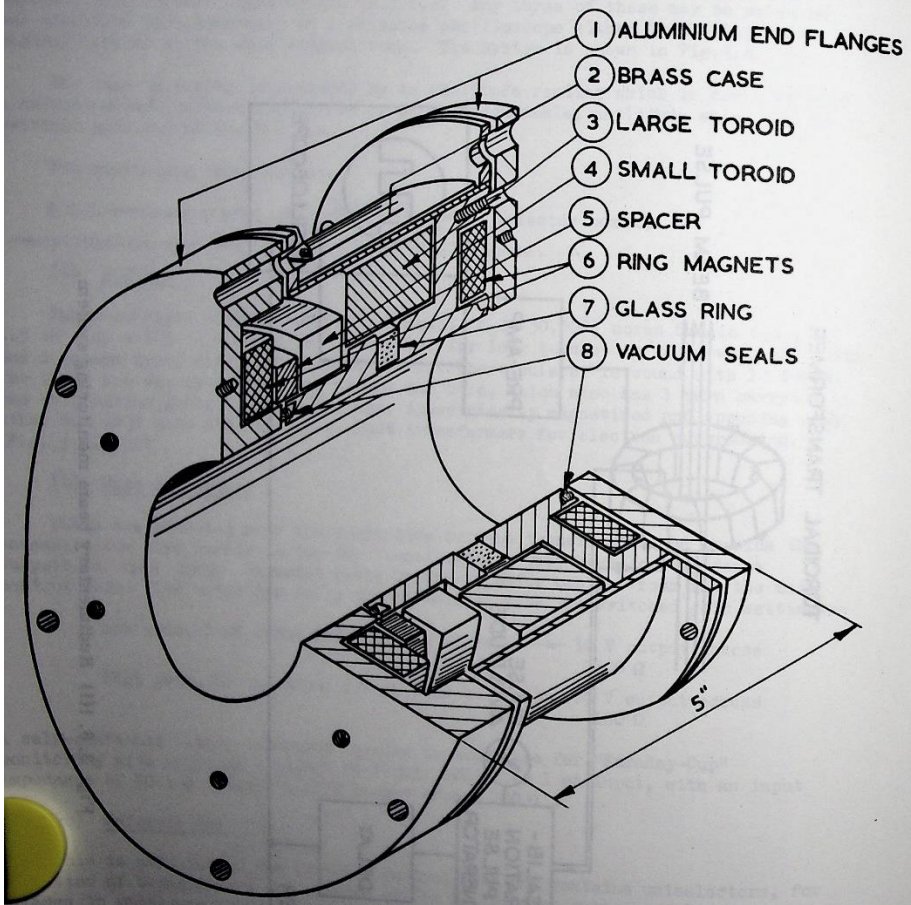

Fig. 3.6.1(ii) Screening mount for beam current transformers.

(d) Calibration Boxes (No. 1, 2 and 3)

These contain transistor circuits for delayed triggering and for the generation of the calibration pulse. The controls provided give –

Control of the calibration pulse currents; direct reading of the beam amplitude by a meter; variation of the calibration pulse time delay with respect to a standard trigger pulse input; control of the pulse length; 3-channel selection of the B.C.T.s; selection of the calibration pulse route; monitor outputs; and fault and warn indication using uniselector operation indicators.

The calibration pulse characteristics are –

Amplitude continuously variable (4 ranges)	10 μA to 100 mA
Accuracy	±2%
Pulse length	100 μs or 2.5 ms
Delay with respect to the input trigger	10 μs to 10 ms.

The response of the complete system to a 2 ms rectangular beam pulse is limited by the amplifier output stage and the balance/unbalance transformer. The rise and decay times are less than 2 μs and the pulse droop is not greater than 5%.

Operational Experience and Projected Future Development

The system has been developed steadily since it was first used some two years ago. Points of particular interest are:-

(i) zener diode stabilisers in each head amplifier to eliminate inter-toroid coupling when using one central power supply,

(ii) symmetrically disposed windings and external magnetic screens at the B.C.T.s to reduce the effect of external magnetic fields (50 c/s),

(iii) gold-plated uniselector contacts for improved low level operation,

(iv) magnetic screening of the balance/unbalance transformers.

To date, no trouble has been experienced from radiation damage to the head amplifiers and even with prolonged operation at full beam intensity, adequate life is anticipated. (Deterioration of the head amplifiers does not affect the accuracy of the measurement).

Measurements of beam current pulses with intensities less than 100 μA can be taken on any of the B.C.T.s and intensities of less than 10 μA can be monitored where magnetic screens have been fitted.

Modifications are in hand to improve the speed of the system. It will then be possible to monitor beam pulses of 300 ns with rise-times of the order of 100 ns. This accuracy is adequate for timing purposes.

3.6.2. Timing Facilities

A comprehensive fully transistorised timing system is proposed for the injector. This will allow maximum flexibility for experimental and commissioning purposes and apply minimum restriction to the main machine. The system has not yet been finalised but most of the basic units have been in use for some time.

The system uses pulses from the magnet field integrators, to provide timing information for 'acceleration cycles', and pulses derived from the main alternators, to enable parts of the injector to be run at multiples of the magnet pulse repetition frequency.

A description of the system is given in (18).

(a) Master Timer

The master timer, controls the gating of the pulses from the field integrators and from a counter chain locked to the magnet timer circuits. Provision is made for synchronised, single-shot operation of the magnet/injector (i.e. one magnet cycle synchronised with continuous pulsing of the injector) and for normal, unsynchronised, single shot. The master timer also contains a pulse generator for injector operation without the magnet.

(b) Delay Boxes

The delay boxes provide accurate, jitter-free, directly calibrated delays which are required for correct sequential operation of the injector equipment. Three independant delayed outputs are derived from each of four inputs. The delays introduced are directly proportional to the potential difference from the slider of a helipot, which is fed from a stabilised supply to earth. This approach was adopted to reduce to a minimum, the number of pulses interchanged between the injector control room and the main control room. The delays can be adjusted in the injector and main control rooms and by using a portable extension box in either control room.

The specification for the delay boxes is as follows:-

Input pulse - positive going, 20 V ± 3 V, rise time < 1 μs, pulse length 5-50 μs, input impedance 10 kΩ ± 5%, (or, with the remote input pulse monitor connected, 5 k Ω ± 5%), minimum trigger level 10 V.

Output pulse - positive going, 20 V ± 0.5 V, rise time < 1 μs, pulse length 10 μs ± 2 μs, output impedance ≯ 100Ω , decay time 5 μs ± 2 μs. This is the standard trigger pulse used throughout the injector timing circuits. Delay and jitter on the 10-100 μs range and the 100 μs-1 ms range is ± 0.1 μs; on the 1 ms-10 ms range it is ±1 μs.

(c) Extraction Trigger Control

Using the standard trigger pulse, the extraction trigger control provides the following facilities:

(i) Square pulse of defined length, 20 μs-2.5 ms (main extraction trigger),

(ii) Square pulse of defined length, 20 μs-200 μs (pilot beam trigger),

(iii) Selection of (i) and/or (ii) as required,

(iv) Premature termination of the extraction pulse (beam 'axe')

(v) Suppression of (i) (extraction 'lock-out')

(d) Light Guide System

The light guide system is described in section 3.3.4.

Monitor channels to the Main Control Room

In addition to the monitoring and timing facilities already discussed, it is proposed to use a number of emitter follower units in the injector control room to provide low impedance circuits to the main control room. These units will have the following characteristics:-

There will be six channels (5 emitter followers and 1 direct link),

Input impedance ≏ 100 kΩ for normal input and ≏ 50 kΩ for fast input,

Output impedance - low (dependant upon input resistance).

Gain from the injector to the main-control room will be 0.5 (adjustable over a small range);

With a 2 ms pulse, the rise and decay times for normal input will be ≏ 2 μs, with fast input ≏ 0.1 μs;

Droop ≯ 5%. The maximum input pulse amplitude will be ±40 V with separate plug-in boards for each polarity, maximum input d.c. level, ±350 V. Connection to the main control room will be via a 100Ω terminated cable.

3.6.3. Auxiliary equipment

Auxiliary equipment for the injection system is discussed in the relevant sections elsewhere in this report:

Injector vacuum system	. . .	Section 8.11
Injector control system	. . .	Section 9.1
Injector vacuum controls	. . .	Section 9.2.2
Injector auxiliary plant	. . .	Section 10.8

3.7. Beam Experiments

3.7.1. Emittance Definition in LEDS

A system of quadrupole triplets and defining apertures was set up in the LEDS with a view to defining the emittance (phase-space characteristics) of the beam entering the linac. The experiment confirmed the theoretical predictions of displacement acceptance but revealed a discrepancy as far as divergence is concerned. This will be investigated further.

3.7.2. Momentum Analysis

Momentum analysis of the 15 MeV beam has been carried out using one of the sector magnets which is used in the inflector system, in a temporary set up. The magnet is a 50°, 70 cm radius element, which, used with 1 mm wide slits, gives a resolution of about 40 keV.

A series of momentum spectra, taken at different field levels, is shown in Fig. 3.7.1(i). The graphs (a) to (f) may be compared with the spectrum computed for a 30° synchronous phase angle, shown in graph (g), and satisfactory agreement can be seen with the spectrum obtained at a 7.8 V monitor pulse height.

The way in which the momentum distribution should vary with field level can be deduced from Fig. 3.7.1(ii). This shows the computed energy-phase distribution of protons at the linac output and is for 30° synchronous phase angle, giving 2.65 linear phase oscillations. The effect of changing the linac field level is to change the number of linear phase oscillations and effectively to produce a rotation of the energy-phase curve. For example, for a integral number of half linear phase oscillations the momentum-spectrum would have a strong central peak, while for an odd number of quarter phase oscillations it would have two prominent, widely spaced peaks separated by a plateau. These expectations are in broad agreement with the observed spectra. A similar set of spectra obtained for various linac field tilts show that the predominant effect of field tilting on the momentum distribution is also one of a change in the number of phase oscillations.

3.7.3. Emittance Measurements

A series of measurements of the emittance of the 15 MeV beam is being carried out in the HEDS. Information which relates the output emittance to the settings of the linac quadrupoles, is required before the tank focusing can be set correctly.

Because of limited aperture in the HEDS flight-tube, the normal method of measuring emittance with two movable slits is not feasible. A system has been worked out, see Fig. 3.7.2(i), using a steering magnet and a fixed central slit, to replace either or both of the movable slits. This system overcomes the aperture limitation sufficiently.

It can be shown that on the phase space diagram at the output end of the linac -

(i) the lines corresponding to a constant value of 'd' (see Fig. 3.7.2(i)), have a slope of $1/l_1$ and cut the θ axis at $-dl_2/l_1 l_3$

(ii) the lines corresponding to a constant value of magnet current 'I', have a slope of $\frac{-1}{l_1+l_2}$ and cut the r axis at $-KIl_2$

(600 keV INJECTION ENERGY AND NOMINALLY FLAT FIELD)
GRAPHS (a)-(f) EXPERIMENTAL : PARAMETER IS MONITOR VOLTAGE PROPORTIONAL TO LINAC FIELD LEVEL
GRAPH (g) COMPUTED : CURRENT PER 50 keV INTERVAL FOR MOTION ON AXIS AT 30° SYNCHRONOUS PHASE ANGLE.

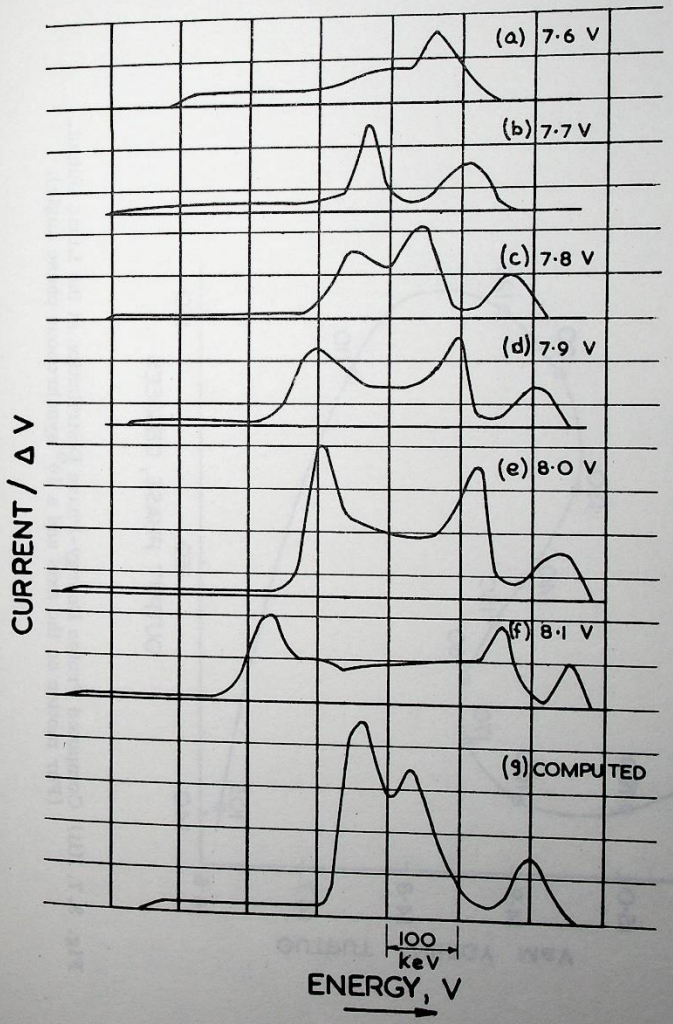

Fig. 3.7.1(i) 15 MeV Momentum Spectra at Various Linac Field Levels.

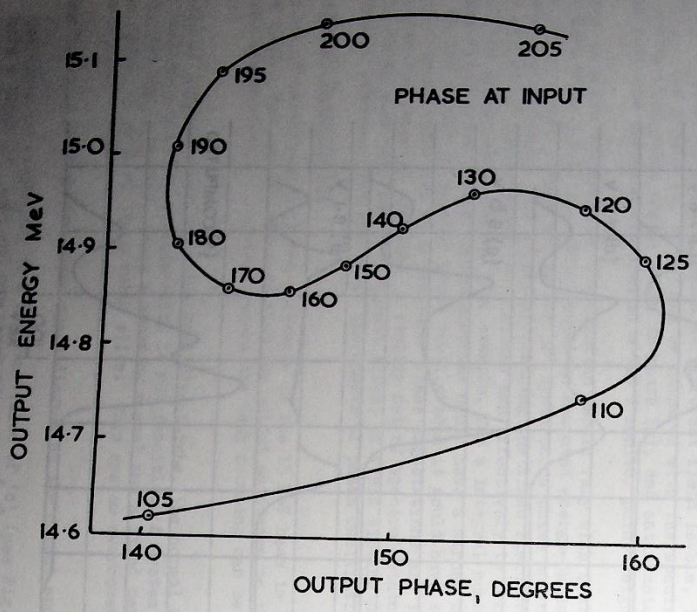

Fig. 3.7.1(ii) Computed Proton Energy-Phase Distribution at the Linac Output. (For motion on the axis and a 30^{o} synchronous phase angle).

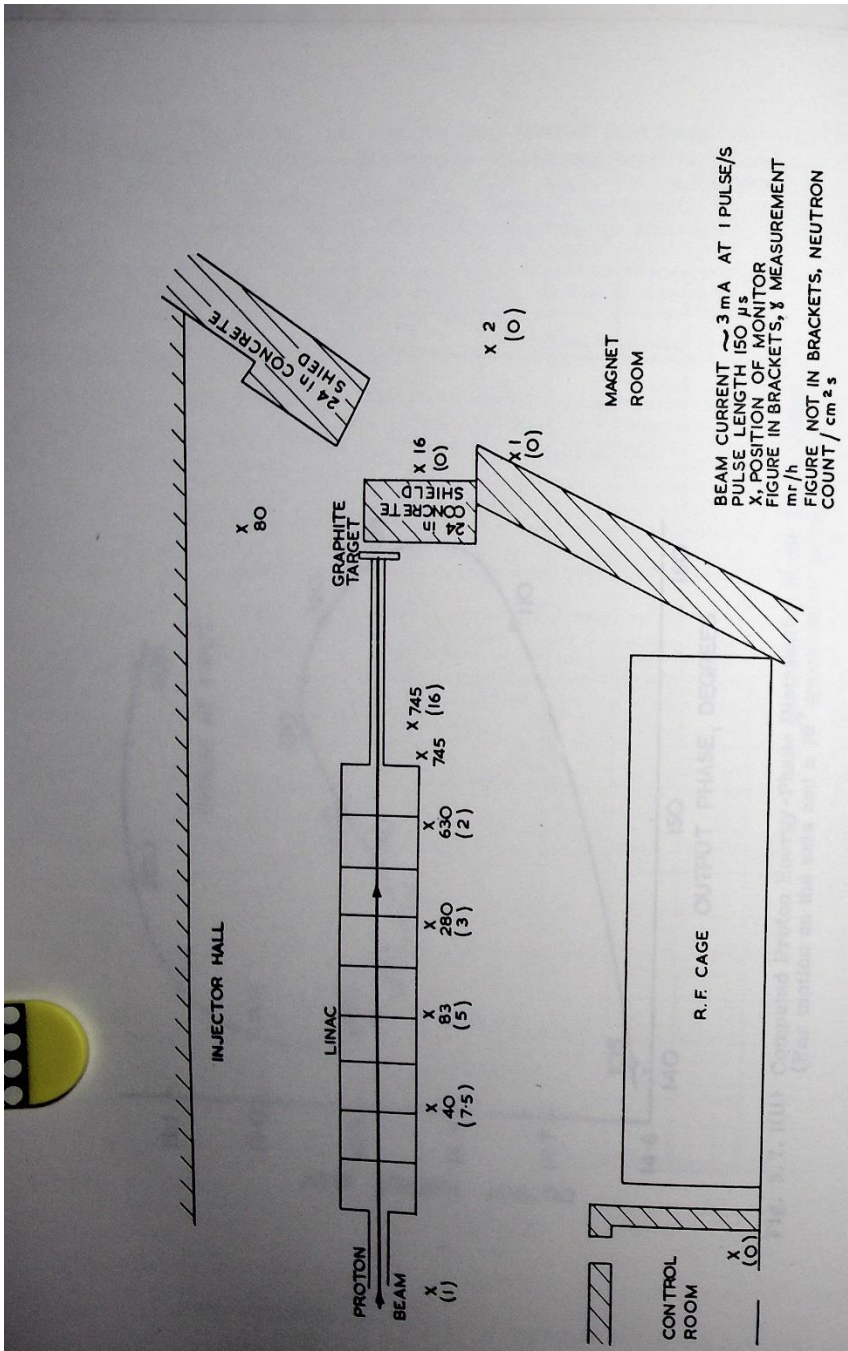

Fig. 3.7.3(i) Map of observed gamma and neutron levels (September 1962).

Fig. 3.7.2(i) Emittance Measuring System.

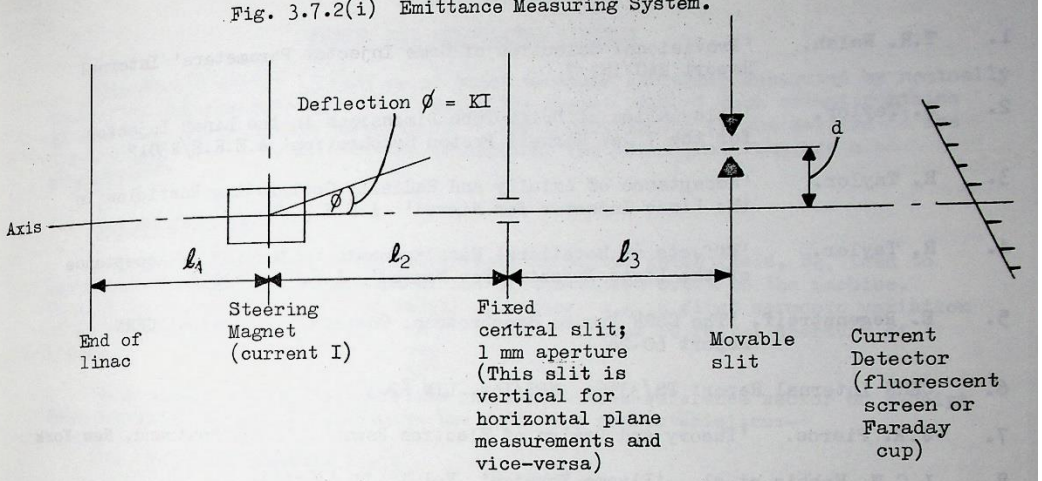

Charts have been prepared for both the horizontal and vertical planes on which the beam extinction settings of "d" and "I" can be plotted to give the linac output beam emittance diagram directly. Using the same equipment but a modified technique it is possible to plot current density profiles in the linac output phase space ellipse.

Further work remains to be done on the HEDS emittance measurements and on setting up the linac quadrupoles.

3.7.4. Radiation Survey

Fig. 3.7.3(i) is a map showing some observed gamma and neutron levels. The levels appear fairly reproducible, but the neutron flux, obtained from measurement of induced activity in Indium foils is subject to variations from run-to-run which are not at present properly understood. As far as possible, all surfaces in the HEDS, which are intentionally introduced so as to intercept the beam are of graphite, whose p-n production threshold is approximately 18 MeV. The drift tube bores from drift tube No.35 upwards are also lined with 1 mm thick graphite sleeves. Provision has been made to line the remaining drift tubes at a suitable opportunity.

At present levels of operation the integrated dose is nowhere excessive but when the injector is running at its design current and at full duty cycle, the neutron levels are expected to exceed tolerance in the vicinity of the 15 MeV beam.

REFERENCES FOR SECTION 3

1. T.R. Walsh. 'Provisional Selection of Some Injector Parameters' Internal Report HAG/INJ/7

2. R. Taylor. 'Calculation of Drift-Tube Dimensions in the Linac Injector for the 7 GeV Harwell Proton Synchrotron' A.E.R.E/R3012

3. R. Taylor. 'Acceptance of Axially and Radially Oscillating Particles in the Linac Injector for Nimrod' A.E.R.E./R3013

4. R. Taylor. 'Effects of Rotational Misalignments on the Radial Acceptance of the Linac Injector for Nimrod' A.E.R.E./R3096

5. E. Regenstreif. 'The CERN Proton Synchrotron. Chapter 5 Injection' CERN Report 60-26

6. CERN Internal Report PS/3396; MPS/Int. LIN 62-3

7. J.R. Pierce. 'Theory and Design of Electron Beams' D. Van Nostrand, New York

8. L.C.W. Hobbis et al. 'Plasma Physics' Vol.1, pp 130-134.

9. J.J. Wilkins. 'Design Notes on Resonators on Proton Linear Accelerators' A.E.R.E. GP/R1613

10. N.D. West. 'R.F. Model Measurements for the Injector Linac' Internal Report HAG/INJ/11.

11. J.T. Hyman. 'Design of Quadrupole Focusing Magnets' Internal Report HAG/INJ/9.

12. J.T. Hyman. 'Quadrupole Dimensions for the Synchrotron Injector Linac'. Internal Report HAG/INJ/12.

13. J.T. Hyman. 'Modified Design and Dimensions for the Injector Linac Quadrupoles' Internal Report HAG/INJ/14

14. R. Billinge. 'Beam Steering in the Nimrod Injector System' Internal Report HAG/INJ/16

15. J.T. Hyman. 'Some High Current Circuits Using Transistors' NIRL/R/17

16. R. Billinge. 'An Achromatic Inflector System for Nimrod' AERE/R3475

17. M. Bell. 'Injection into the 7 GeV Synchrotron' AERE/T/M155

18. J.T. Hyman. 'Injector Control Room Pulse Timing System' Internal Report HAG/INJ/24.

SECTION 4

MAGNET AND ASSOCIATED SYSTEMS

The Nimrod magnet is made up of eight sections (octants) separated by nominally field-free regions (straight sections). The magnet yoke of each octant contains 42 sectors. Early design information(1) and a description of the sectors(2) are already available. Details of the foundations for the magnet ring are also published(3).

4.1. Sector Testing

It can be shown that azimuthal variations of the guide field, B_z, lead to variations in the radial position of the proton closed orbit in the machine. This is equivalent to a loss of radial aperture; e.g. a first harmonic variation of B_z with amplitude $\frac{\Delta B_z}{B_z} = \frac{4}{10^4}$ leads to a loss of radial aperture of 1 inch.

Each magnet sector was therefore compared with a reference sector on receipt from the manufacturers to determine the following characteristics:-

(i) Value of remanent field

(ii) Relative values of field produced by current in the energising coils at values of field in the gap varying from 200 to 14,000 gauss

(iii) Eddy current effects.

The electronic measuring equipment(4), the model (see Fig. 4.1(i)) and its power supply have been described elsewhere(5). The measurement programme took about sixteen months.

4.1.1. Results of Tests

Variations in the value of the remanent field and hence the value of gap field at low pulsed fields were the most noticeable. Fig. 4.1(ii) shows the value of the remanent field plotted against the order in which the sectors were manufactured. It is very noticeable that early sectors had a very much higher remanent field (up to 24 gauss) than later sectors. This was due to the fact that it was not possible to manufacture the whole quantity of steel in one batch and randomise completely. The steel which had been annealed early in the programme was the cause of the high remanence and was present in sectors up to about number 245.

The largest variation in relative field at low fields was directly due to variations in remanent field values. This is shown on Fig. 4.1(iii) which has a band containing the result of plotting relative fields at 200 gauss against remanent field. The width of the band was about 1.3%, or 2.6 gauss, compared with a remanent field band of 12 gauss. This graph also shows the interdependance of remanent field and low field permeability; viz, sectors with high remanent field have low permeability and hence relatively low pulsed field values at low fields.

There were differences in remanent fields measured for a given sector with the high and low dB/dt at low fields. In general the remanent fields of all sectors were lower with the higher dB/dt, and sectors with low remanent fields were depressed more at the higher dB/dt.